Table of Contents

1 Background

1.1 Introduction and Motivation

Fast moving floodwaters are a major hazard to the public, emergency services, vehicles and property. Extreme flood events can lead to large numbers of casualties and severe economic damage. Flooding has recently affected Britain in the Winter Storms of 2013/2014 causing 17 fatalities, whereas global flooding can cause much more widespread damage. A relevant example for this project is the 2004 Indian Ocean Tsunami, which killed 227,000 people (Athukorala, (2012)). The risks of people and vehicles being caught in fast moving floodwaters are likely to increase in the future due to the globally increasing urban population (especially in flood-prone areas) creating more severe rainfall runoff and flash flood events. Climate change is also causing meteorological change, resulting in an increase in flash flooding events, according to the IPCC (IPCC (2007)). This has led to flood risk management becoming a major area of study, of which a small part is concerned with the stability of humans and vehicles in floodways. Floodways have been defined as “areas of high velocity and depth of flow where the flood hazard is high”, (NSW government (2007)).

Some specific examples of why it is important to understand the threshold of instability for humans and vehicles in floodways are:

1. Urban flood modelling could predict flood characteristics, which, when combined with the derived stability criterion, can enable estimates of the number of casualties in different areas. Evacuation plans can then be developed with more confidence, potentially saving lives.
2. A vehicle stability criterion would enable estimates of economic damage to vehicles due to a flood. This would be potentially useful for national governments and insurance companies.
3. Instability criteria can be used to determine hazard warnings for storms and flooding events.
4. Safe conditions for emergency service personnel who are working in floodwaters can be specified.

The stability of humans and vehicles in floodways is determined by many factors, two of the most important are the height and velocity of the flow. There are two mechanisms of instability for humans in moving floodwaters: toppling and sliding. Sliding will occur in shallow, fast moving flows and toppling will occur in deeper, slower flows. For vehicles, sliding is the dominant mechanism, however rolling or floating could occur at either extreme of velocity.

1.2 Aims

The main aims of my experiment are to:

1. **Propose quantitative human stability criteria in steady flow, and verify against previous studies.**

This will involve completing a theoretical analysis of human stability in floodways and then using scaled models of humans (of three different sizes) in an experimental study.

2. **Investigate the effect of posture on human stability in floodways.**

Human posture will greatly affect stability, previous scale model studies have not investigated its effects. The posture of a human is a broad topic, which should be approached sytematically.

3. **Propose vehicle stability criteria in steady flow, and verify against previous studies.**

Another experiment will investigate vehicle stability in floodways using various scaled models in a steady flow water flume. A critical velocity-depth curve of stability will be developed and validated in comparison to previous similar studies.

4. **Investigate the effects of bed friction and orientation on vehicle stability.**

To build a more comprehensive understanding of the factors that affect vehicle stability in floodways.

1.3 Literature Review

1.3.1 Human Stability

There have been many varied studies conducted into the stability of humans in floodways, including purely theoretical investigations, scaled model experiments and full scale experiments using real human subjects. Studies that are important to the context of this report are summarised below.

"New criterion for the stability of a human body in floodwaters", Xia et. al., (2014).

This study proposes a theoretical formula for the stability of a human using a force balance analysis and then goes on to a scaled model experiment. Xia et. al. (2014) is very relevant to the current investigation, especially in the approach to the theoretical analysis. It also provides a good starting point with which to compare obtained experimental results, since it employs similar methodology. However, Xia doesn't consider changing human posture, changing bed friction coefficient or changing the model size, all of which will be investigated in detail by this study.

"Human Stability in a High Flood Hazard Zone", Abt et. al., (1989).

Abt et. al. (1989) is the first example of a full scale experiment using real human volunteers. They firstly used a human sized model and subsequently 20 human subjects to determine their critical stability profiles. The results (as for most of the human stability studies) are presented as an equation relating the product of the critical depth and velocity to the human's height (*L*) and mass (*m*). Abt et. al. (1989) published the following equation:

$$hv_c = 0.0929(e^{0.001906Lm+1.09})^2 \quad (1)$$

Abt et. al. (1989) enables a direct and interesting comparison between small scale model experiments and real life human stability to be made. It offers an approximate upper limit on the human stability, whereas Xia et. al. (2014) offers a lower (more conservative) estimate. It is hoped that (by varying the posture of the scale model to be more stable than Xia et. al. (2014)) my study will produce a set of results somewhere in between the two.

"Hydrodynamic Models of Human Stability in a Flood", Lind et. al. (2004).

A theoretical study was carried out by Lind et. al., who used three shapes (circular cylindrical, square cylindrical and cylindrical composite) to approximate humans in floodways. Since it is theoretical, it offers a different perspective on human stability and it is insightful to compare to the scale model and full size model experiments.

Other studies that will be referenced throughout this report are Karvonen et. al. (2000), who used seven real human subjects; Takahashi et. al. (1992), who conducted scale model experiments; and Jonkman et. al. (2008), who assessed the risk of loss of life due to floods.

1.3.2 Vehicle Stability

Vehicle stability in floodways has also been the subject of numerous studies, the most important, in the context of this investigation, are outlined below.

"Criterion of vehicle Stability in floodwaters based on theoretical and experimental studies", Xia et. al. (2013).

Xia et. al. (2013) describes a very similar theoretical analysis to Xia et. al. (2014) (the investigation into human stability). A laboratory experiment based on two model vehicles with three different orientations (0°, 90° and 180°) is then performed, with the results used to propose a vehicle stability criterion. Xia et. al. (2013) uses similar sized scale models and methodology to the current investigation and therefore acts as a suitable study to compare initial results. Xia et. al. (2013) also investigates the effect of ground slope on vehicle stability, and finds a 1:50 ground slope will reduce the critical velocity substantially, especially at low depths.

"Safety Aspects of the Design of Roadways as Floodways", Keller and Mitsch, (1993).

Keller and Mitsch produced a purely theoretical study on the stability of vehicles in floodways. Their process was to calculate the centre of buoyancy and weight distribution at incremental depths (from detailed manufacturer specifications), in order to find the reaction forces. These could then be used, by using a force balance for the equilibrium of sliding, to determine vehicle stability criteria.

Other studies of note are: Shand et. al. (2011), who summarised important studies and collated their results into a conservative stability curve and Bonham et. al. (1967), who produced one of the first investigations into vehicle stability using scaled models.

2 Theory and Experiment Design

2.1 Depth Averaged Velocity

It was only possible to measure the surface velocity of the flow in the experiment. To convert this to a depth averaged velocity (which is required for a comprehensive analysis), a logarithmic boundary layer profile is assumed as shown in Naulluri and Featherstone (2001) pg. 181, and which is taught in the 3D5: Water Engineering module at Cambridge University Engineering Department (CUED). Firstly, it was necessary to determine whether the flow regime is hydraulically smooth or hydraulically rough in the wave flume. A modified version of Moody's diagram was used, see Figure 1, where R_h is the hydraulic radius of the flume, k_s is the representative roughness height, v is the kinematic viscosity of water (=10^{-6} m^2s^{-1}) and U is the flow velocity. Representative roughness height (k_s) was taken to be 0.25mm for scratched steel, as suggested by Flack and Schultz (2010). The two potentially "hydraulically smoothest" results have been plotted on the Moody Diagram in Figure 1 and are located in the transition zone, therefore all results shall be treated using the hydraulically rough regime equation.

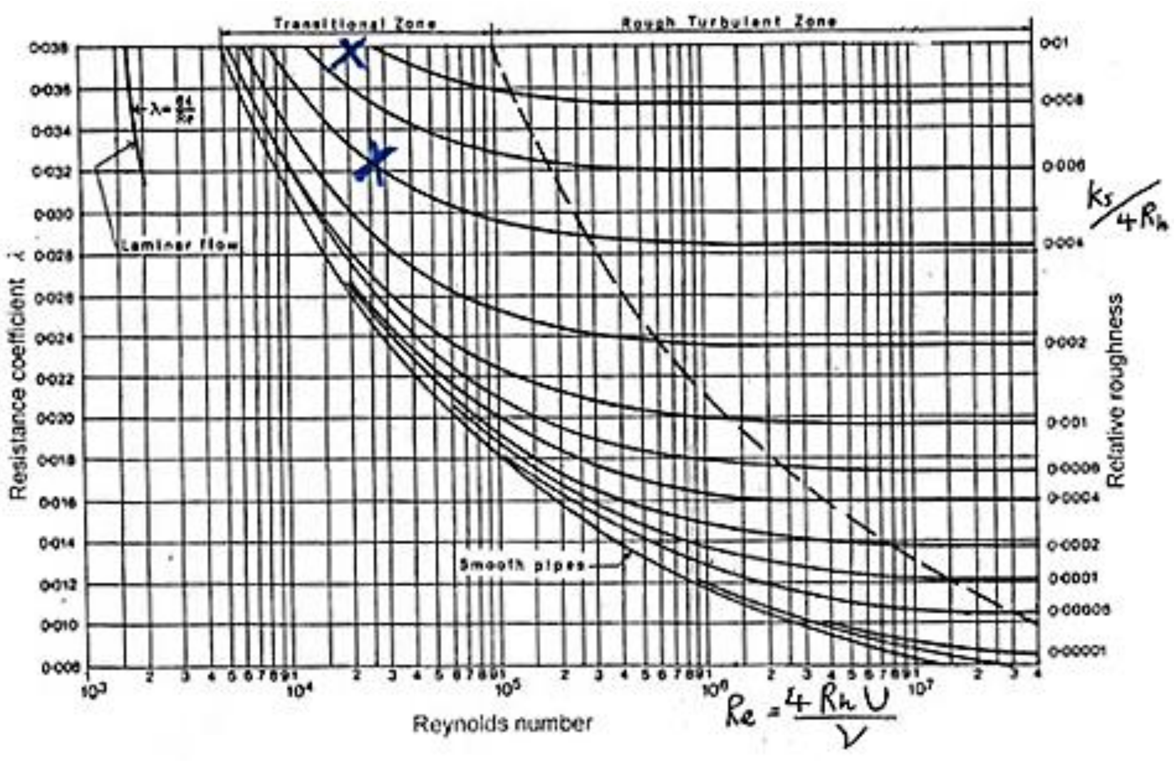

***Figure 1** Moody diagram used to determine the flow regime,* taken *from 3D5 Water Engineering Databook.*

The equation for fully developed boundary layer flow with a free surface in a hydraulically rough regime is given in the databook for module 3D5: Water Engineering, as is shown below:

$$\frac{\overline{u}(z)}{u_*} = \frac{1}{\kappa} ln\left(\frac{30z}{k_s}\right) \quad (2)$$

The process of finding the depth averaged velocity is thus:

1 Find u_* using the depth and velocity of the free stream (which is measured in the experiment),

2 Find $\overline{u}(z = h/e)$, which is then taken as the depth averaged velocity *U.*

All recorded velocities were converted to a depth averaged velocity before being displayed in the results sections below. The conversion must happen before the scaling up of the depths and velocities.

2.2 Dimensional Analysis

In order to scale the model parameters to full human size correctly a dimensional analysis approach was used. The parameters that are considered to affect vehicle and human stability are:

$$v_{crit} = f(h, \rho_m, \rho_w, \nu, g, \theta, d, \mu_{fric}, posture) \quad (3)$$

For clarity, the definitions of the parameters in the equation above are listed in Table 1:

Table 1 *Parameters affecting vehicle and human stability in floodways*

v_{crit}	Critical velocity at instability	g	Acceleration due to gravity
h	Height of flow	d	Height of model
ρ_m	Model density	θ	Slope angle
ρ_w	Water density	μ_{fric}	Friction Coefficient
ν	Kinematic viscosity	Re	Reynolds number

Posture is a broad term that includes the projected area normal to the flow direction and other factors of the model that affect stability such as base width or centre of gravity.

There are 10 parameters and three dimensions, therefore (using Buckingham's Pi Theorem) seven dimensionless groups can be formed from Equation (3). These could be formed as shown in Equation (4):

$$\frac{v_{crit}}{\sqrt{gh}} = f'(\frac{h}{d}, \frac{\rho_w}{\rho_m}, Re, \theta, \mu_{fric}, posture) \quad (4)$$

These dimensionless groups are then either controlled or neglected in the experiment:

1. To control the density ratio, the model with have to be weighted. Therefore mass will be added to the model until the models density is equal to that of a human.

2. Bed slope (θ) is assumed to be small and can therefore be neglected. However, the effect of θ was investigated in detail by Xia et. al. (2013), whose results will be discussed in the context of this experiment (see Section 5.2).
3. The coefficient of friction (μ_{fric}) will also have to be controlled and should be similar to a representative real life value, which is discussed in further detail (see Section 3.2.1.4).
4. The Reynolds Number (*Re*) affects drag coefficient (C_d). C_d is independent of *Re* for $Re > 2x10^4$, as shown by Chanson (2004). Reynolds number is commonly defined as:

$$Re = \frac{vD}{\nu} \tag{5}$$

   Using representative values for humans in floodwaters (*v = 0.5* ms^{-1}, *D = average body width exposed = 0.25 m, v = kinematic viscosity =* 10^{-6} $kgs^{-1}m^{-1}$) returns a Reynolds number of $1.25x10^5$. Therefore is can be assumed that drag coefficient is constant and the same for both the model and real size human. Since C_d is part of a free parameter to be calibrated with the experimental data, an exact numerical value does not need to be determined. For context, values for C_d of approximately 1.5 were adopted for previous studies (e.g. Keller and Mitsch).
5. Posture (including projected area) will be controlled carefully and its effects investigated in detail for both vehicles and humans.

The dimensional analysis (Equation (4)) also gives the scaling factors required to scale the model results to full human size results,

$$\lambda_H = \lambda_L \ , \ \lambda_V = \sqrt{\lambda_L} \tag{6}$$

Where λ_L is the scale ratio of the model size to real size, λ_H is the scale ratio of water depth and λ_V is the scale ratio of flow velocity. These principles drive the general experimental procedure for both the stability of vehicles and humans. Detailed describtions of apparatus and methodology can be found (see Section 3.2) for vehicles and (see Section 4.2) for humans.

3 Vehicle Stability in Steady Flow

Vehicle stability is considered here first because the human stability experiment only builds on the theory, apparatus and method employed for investigating vehicle stability.

3.1 Vehicle Stability Theory: Force Analysis and Formula Derivation

To ensure a comprehensive analysis of vehicle stability in steady flows, a theoretical approach was undertaken first.

An analysis of the forces acting on a partially submerged vehicle in a floodway is presented below. This theoretical analysis aims to produce an equation for the critical velocity required to induce motion by considering the equilibrium of sliding of the vehicle. It is assumed that the vehicle's wheels are locked against motion and that the vehicle is watertight for a short period of time as the flood builds up. More information and detail on some aspects this force analysis can be found in Xia et al. (2011).

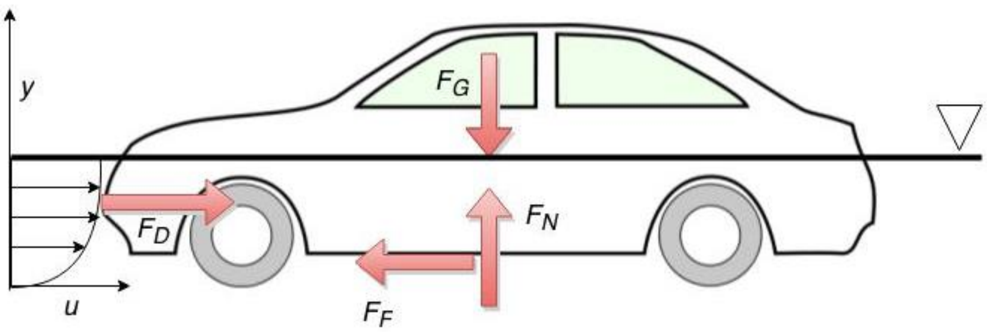

Figure 2 *Forces acting on a partially submerged vehicle in a floodway*

Although this analysis only considers sliding instability, it should be noted that there are two other modes of instability, namely floating and rolling. Floating will occur when the effective weight drops to zero, which can only occur before sliding instability if the flow is stationary. Thus floating instability is unlikely to happen in floodways and will not be considered further. Rolling instability could occur when a very high velocity flow creates a sufficient moment in order to topple the vehicle. The possibility of rolling could be increased by surface flaws (e.g. kerbs or ditches) in the real world, however only a flat surface was considered in this experiment. It is unusual for vehicles to roll in flood waters (Xia et al. (2013)) and was not observed during this experiment, and therefore has not been considered in this analysis.

There are four forces acting on the vehicle, as seen in Figure 2: drag force (F_D), friction force (F_F), effective weight (F_G) and normal reaction force (F_N). The dimensions of the vehicle are described by length (l_v), breadth (b_v) and height (h_v).

3.1.1 Effective Weight

For a partially submerged vehicle, the effective weight is given by:

$$F_G = Al_v b_v (h_v \gamma_v - R_f h_v \gamma_w) \tag{7}$$

Where A is a coefficient for the effective vehicle volume, γ_v and γ_w are the unit weights of the vehicle and water respectively and R_f is given by:

$$R_f = \frac{h_v \gamma_v}{h_k \gamma_w} \tag{8}$$

Where h_k is the floating depth of the vehicle, which can be easily measured in practice using stationary water and a depth gauge.

3.1.2 Drag Force

The drag force acting on an object is given by Equation (9), from (Chien and Wan (1999)):

$$F_D = \frac{1}{2} C_d \rho_w A_d u^2 \tag{9}$$

Where C_d is the drag coefficient, ρ_w is the density of water, A_d is the normal projected area of the object in the flow and u is the near bed fluid velocity. A_d will vary with the detailed shape of the vehicle and it's orientation to the flow and can therefore be given by Equation (10) (for the flow hitting the side of the vehicle):

$$A_d = a_d h_f l_v \tag{10}$$

Where a_d is a coefficient relating to the detailed shape of the vehicle and h_f is the incoming water depth.

3.1.3 Frictional Force

The static frictional force can simply be given by the coulomb model for friction, $F_F = \mu F_N$, where μ is the coefficient of friction between the wet road and tyres of the vehicle. $F_N = F_G$ and therefore:

$$F_F = \mu F_G = \mu(Al_v b_v(h_v\gamma_v - R_f h_v \gamma_w)) \tag{11}$$

3.1.4 Formula Derivation

Now, from the equilibrium of sliding, $F_D = F_F$, and therefore by substitution:

$$u = [\frac{\mu A}{a_d C_d}]^{0.5}.[2gl_v(\frac{h_v\rho_v}{h_f\rho_w} - R_f)]^{0.5} \tag{12}$$

Since u is the near bed fluid velocity (and therefore difficult to determine) it should be transformed into the depth averaged velocity (U) (which is what will be calculated in the experiment). This can be achieved by using a power law relationship (as described in Xia et. al. (2013)) of the form:

$$u_y = (1+\beta)U(\frac{y}{h_f})^{\beta} \tag{13}$$

Where u_y is the fluid velocity at height y above the bed, and β is a parameter to be determined by calibration with the experimental data.

Therefore, taking the characteristic depth for the bed velocity as a fraction of h_v, an equation can be determined which relates the critical depth averaged velocity for instability to the incoming flow depth. This equation will depend on A_d and therefore the equation will be different for each different effective projected area. There are three model sizes (small, medium and large) and three characteristic orientations to be considered (0°, 45°, and 90°), so nine different effective projected areas to consider. The 135° and 180° orientations have the same projected area as the 45° and 0° orientations respectively. So combining and rearranging Equation (12) and Equation (13) yields Equation (14) (for the case of 0° (head on) flow):

$$U_c = \alpha\left(\frac{h_f}{h_p}\right)^{\beta}\sqrt{2gb_v\left(\frac{h_v\rho_v}{hf\rho_w} - R_f\right)} \tag{14}$$

For the case of flow at 90°, Equation (14) can be modified to produce Equation (15):

$$U_c = \alpha\left(\frac{h_f}{h_p}\right)^{\beta}\sqrt{2gl_v\left(\frac{h_v\rho_v}{hf\rho_w} - R_f\right)} \tag{15}$$

For the case of flow at 45°, Equation (16) is produced:

$$U_c = \alpha \left(\frac{h_f}{h_p} \right)^{\beta} \sqrt{2g(b_v \sin 45 + l_v \sin 45) \left(\frac{h_v \rho_v}{h f \rho_w} - R_f \right)} \qquad (16)$$

These three equations will be used to determine the parameters α and β using linear regression with the experimental data. The equations essentially represent the shape of the curve to be fit to the experimental data.

The parameter α (shown in Equation (17)) depends on *μ*, C_d, *A* and a_d. It is therefore affected by factors such as detailed vehicle shape and bed roughness.

$$\alpha = \sqrt{\frac{\mu a_c}{C_d a_d}} [(1 + \beta)(a_b)^{\beta}]^{-1} \qquad (17)$$

3.2 Apparatus and Experimental Techniques

3.2.1 Apparatus

Detail of the apparatus that was used for the vehicle stability experiments is below.

3.2.1.1 Wave Flume

The investigation will use the Engineering department's small wave flume, with dimensions 4m long, 0.25m wide and 0.50m high and situated in the Hydraulics Laboratory. It is capable of achieving a maximum bed slope of 1:25 and also has the capacity of attaching a 20cm high "end plate" which can increase the depth of flow somewhat independently of velocity. This leads to three factors affecting the flow conditions (water depth and velocity): bed slope, flow rate and end plate height, finding a combination that gives suitable depths and velocities can be extremely difficult. The flume has problems achieving high velocities at low depths, this is discussed further (see Section 5.1), and it also narrow enough to create near wall effect problems for most models (see Section 5.1.1).

3.2.1.2 Measurement Apparatus

Flow depth was measured using a needle depth gauge, shown in Figure 3. With a precision of 0.5mm, it was considered to be accurate to ±1mm although had to be recalibrated every time it was knocked slightly.

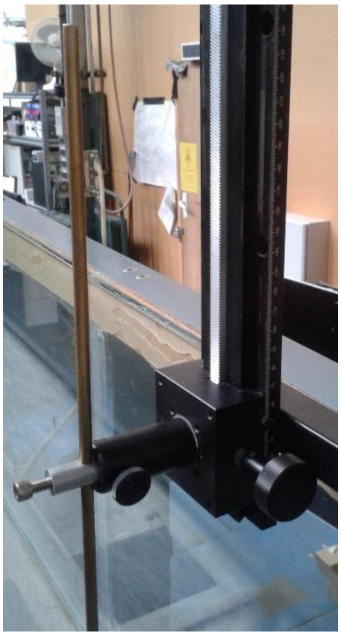

Figure 3 *The needle depth gauge used in the experiment*

A Vectrino Acoustic Doppler Velocimeter produced by Nortek International was available for use, however it requires at least 5cm of water to achieve accurate data, and many of the vehicle experiments were running in sub 2 cm depth. A simple method of timing a small float to traverse an appropriate length of flume was adopted. There are significant problems with this method however: only free stream velocity is recorded (no indication of depth averaged velocity), inherent inaccuracy due to the random path of the float down the flume, very time consuming and also possibility in human error in the timing. It was therefore decided to record three times for each measurement to increase the confidence level in the results. A more detailed discussion in presented later (see Section 5.1.2).

Various alternative options were considered for measuring the velocity (or to measure flow rate and convert to velocity). For example the use of a flow rate meter or even measuring the volume of water exiting the flume over a certain time. Due to the setup of the wave flume, these options could not be implemented.

3.2.1.3 Vehicle Models

Three different size vehicle models were used in the investigation, firstly in order to verify the scaling method and subsequently to increase reliability in the posture and orientation investigation.

Figure 4 *The small, medium and large model vehicles in the water flume. Left: small, Middle: medium, Right: Large*

Figure 4 shows the shape similarity between the large and medium models, but the small model shows no shape similarity to the others. Each model had key parameters measured, which are shown in Table 2:

Table 2 *Key parameters for each model*

	Length (l_v) [m]	**Breadth (b_v) [m]**	**Height (h_v) [m]**	**Mass (m_v) [kg]**	**Floating height (h_k) [m]**
Small Vehicle	0.069	0.035	0.033	0.0139	0.020
Medium Vehicle	0.110	0.050	0.036	0.0330	0.022
Large Vehicle	0.150	0.070	0.048	0.0843	0.028

The models had to be modified to ensure that they did not fill with water (see Section 3.1). Silica sealant proved to be ineffective, but shaping a block of water resistant foam to fit the vehicle's internal shape was most effective in preventing water ingress. Wheels were locked against rotation with two-part Araldite epoxy adhesive. Finally, the models had to be weighted in accordance with the dimensional analysis (see Section 2.2) to maintain the density ratio. Real vehicle manufacturer's dimension and weight data was found online for vehicles of a similar shape, a "Daihatsu Move" was selected for the small model whilst a "Chrysler Crossfire" was considered appropriate for the medium and large models. Mass was added in the form steel plates fixed to the base of the vehicles.

3.2.1.4 Materials to Vary Bed Friction

One improvement of this study over previous studies is an experimental investigation into the effect of bed friction on the stability of a vehicle. It is known from the Vehicle Stability Theory (see Section 3.1), that the parameter α is proportional to $\mu^{0.5}$ and the critical velocity U_c is proportional to α.

In order to test this experimentally, three grades of bed surface friction (smooth, intermediate and rough) were investigated. Modifying the surface friction was achieved by using different grades of waterproof sandpaper bonded to the steel base plate in the flume. In order to cause minimal disruption to the water flow, very small areas of sandpaper were used and it was assumed that they would not cause significant changes in the macro flow velocity profile. The friction coefficient of each material was measured using a submerged inclined slope tilted until the vehicle (which had to be weighted) slid down the slope. The results are shown in Table 3:

Table 3 *Bed surface roughness categories and coefficients of friction*

Surface Roughness	Surface Material	Measured Friction Coefficient (μ)
Smooth	Steel	0.35
Intermediate	1200 grade sandpaper	0.42
Rough	320 grade sandpaper	0.60

Bonham and Hattersly (1967), corresponded with road experts and test laboratories to determine that a friction coefficient of $\mu = 0.3$ should be used, and this was considered very conservative for the majority of road and tyre types. A friction coefficient of approximately 0.3 has been adopted in many vehicle stability investigations since, however it is always regarded as very conservative. According to Ludema (1975), the coefficient of friction for vehicles on wet roads can be anywhere from 0.5 to 1.0, depending on the condition of the tyres. It is assumed that the wheels of the small, medium and large vehicles are all made from the same material, and therefore the friction coefficients listed above can be used for all three vehicle sizes.

3.2.2 Experimental Techniques

All experiments were carried out using the apparatus listed in the Apparatus section (see Section 3.2.1). Multiple experiments were run, but they were in three broad areas: Model size investigation, bed friction investigation and orientation investigation. Table 4 shows the experiments that needed to be performed.

Table 4 *Table of experimental results sets that were recorded.*

	Small Vehicle	Medium Vehicle	Large Vehicle
Smooth	0°, 90°, 180°	0°, 90°, 180°	0°
Intermediate	0°, 45°, 90°, 135°, 180°	0°, 45°, 90°, 135°, 180°	0°
Rough	0°, 90°, 180°	0°, 90°, 180°	0°

The 25 sets of data in Table 4 represent 175 individual experiment runs. Each experimental run requires finding the critical point of instability (by very slowly increasing flow rate until failure), then taking measurements of depth and free stream velocity (using the apparatus detailed in the Apparatus section (see Section 3.2.1). Free stream velocity was recorded three times for each run.

In an urban flooding environment, floodwaters could impact a vehicle from any direction and it is therefore important to consider the impact of the orientation of the vehicle on its stability. This study considers five key orientations: 0°, 45°, 90°, 135° and 180°, which are shown schematically in Figure 5 below.

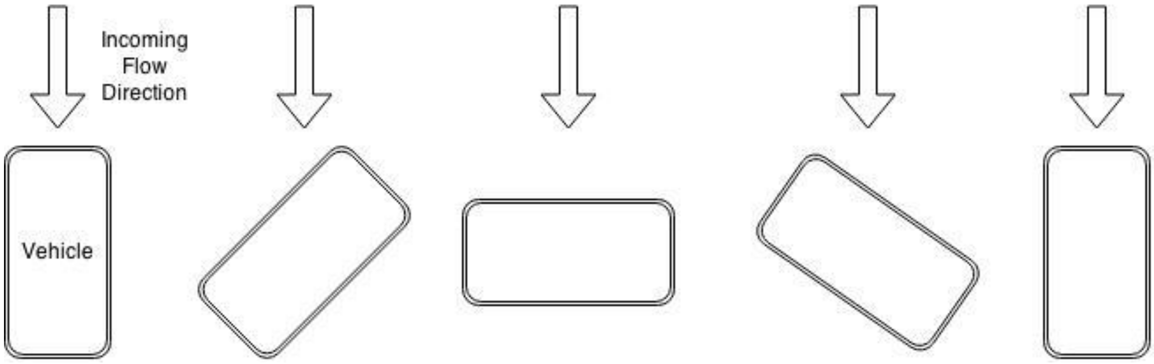

0° 45° 90° 135° 180°

Figure 5 *Showing the geometry of the five different orientations considered in the study*

3.3 Results and Discussion

As explained in the Experimental Techniques section (see Section 3.2.2), Table 4 shows the data sets that were obtained.

3.3.1 Parameter Calibration

As described in the Vehicle Stability Theory section (see Section 3.1), the critical velocity for sliding (resulting from the force balance) results in nine equations representing the combination of three vehicle sizes and three characteristic orientation angles (0°, 45° and 90°). In order to determine the free parameters α and β for each set of results (25 in total), a MATLAB script was written to perform unconstrained non-linear optimization with the MATLAB function `fminsearch`. This script was run using the unscaled, depth averaged velocity data and the shape of the curve that the script was trying to fit was changed each time in accordance with Section 3.1.4. An example curve fitting graph that was produced in MATLAB for the medium vehicle on a rough bed at 90° orientation can be seen in Figure 6. This process was repeated for all results sets in order to obtain α and β.

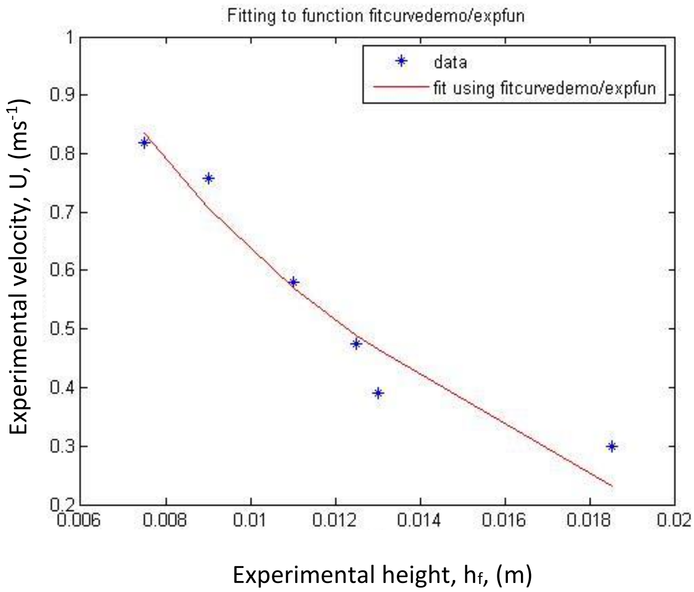

Figure 6 *Example curve fitting and parameter determination using MATLAB*

These free parameters (once determined) can be used to plot appropriate best fit curves for each data set in order to enable clearer comparison between results. All the free parameters for each data set are shown in Table 5.

Table 5 *Parameters in the critical velocity formula for every result set.*

		Small Vehicle		**Medium Vehicle**		**Large Vehicle**	
		α ($m^{0.5}s^{-1}$)	**β (-)**	**α ($m^{0.5}s^{-1}$)**	**β (-)**	**α ($m^{0.5}s^{-1}$)**	**β (-)**
Smooth Bed	**0°**	1.69	0.38	0.74	-0.04	0.39	-0.62
	90°	1.01	0.36	0.37	-0.18		
	180°	1.24	0.17	0.69	-0.18		
Intermediate Bed	**0°**	2.10	0.52	1.81	0.41	1.42	0.28
	45°	1.27	0.50	1.38	0.59		
	90°	1.49	0.60	1.49	0.63		
	135°	1.18	0.44	1.22	0.46		
	180°	1.88	0.40	3.19	0.82		
Rough Bed	**0°**	0.85	-0.37	1.08	-0.09	1.60	0.21
	90°	1.48	0.44	0.62	-0.13		
	180	1.83	0.23	1.67	0.23		

Although broad trends can be seen in the free parameters, there is significant variation as a result of small data sets with fairy large error margins. This is also the cause of some values of negative β (which should not be negative (according to Equation (13))).

3.3.2 Vehicle Size Comparison

A comparison of the stability curves of the three different vehicle sizes is presented in order to validate the scaling method and dimensional analysis. "Stability curves" are the critical velocity-depth relationships, or the upper limit of stability for a vehicle or human. Figure 7 presents stability curves for the three vehicles under smooth bed, 0° Orientation conditions. All results from here on have been scaled to full size using the scaling method derived from the Dimensional Analysis section (see Section 2.2).

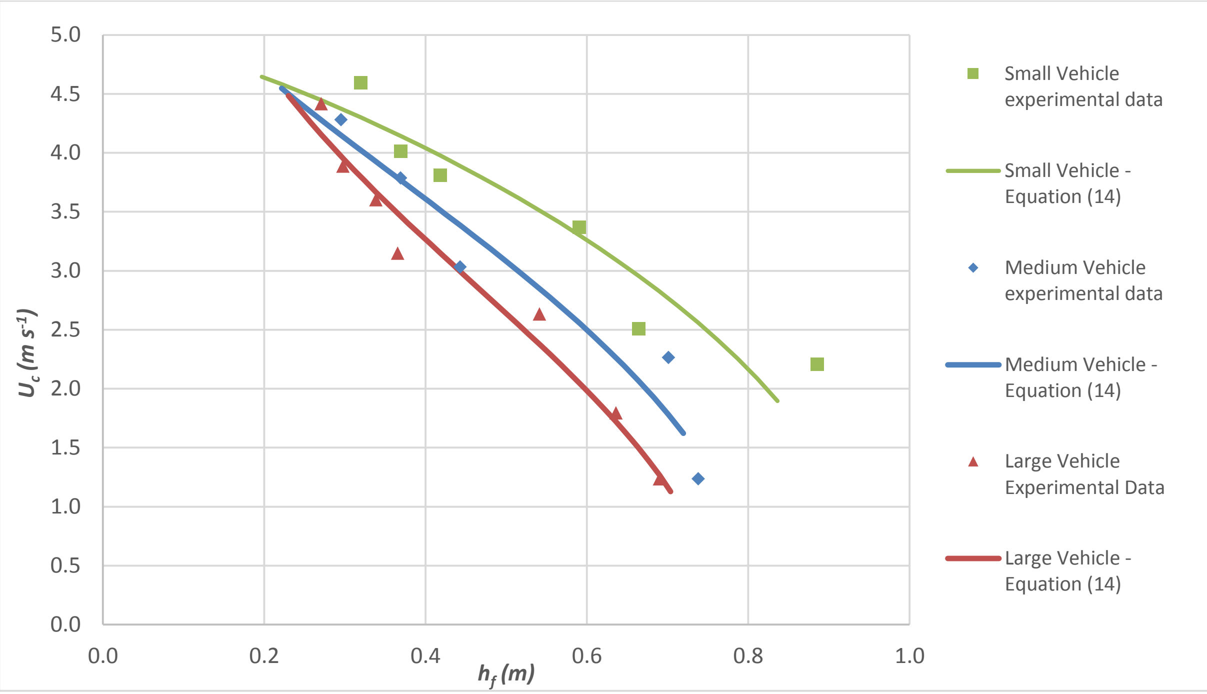

Figure 7 *Stability curves for small, medium and large size vehicles on smooth surfaces, 0° orientation.*

There is good shape similarity between the large and medium vehicles, but poor shape similarity with the small vehicle (see Figure 4). Additionally, the selected real-world vehicle was different for the small and medium/large vehicles (see Section 3.2.1.3), resulting in different density ratios required. It is therefore expected that the small vehicle shows little correlation with the medium/large vehicles in terms of stability curve shape or critical velocity magnitude. The stability curves are expected to be similar for the medium/large vehicles, and Figure 7 justifies this. As the depth is increased, the shape discrepancy of the smaller vehicle becomes more apparent (since the small vehicle has a more rectangular frontal shape compared to the other vehicles) which results in the divergence of the stability curves.

Figure 7 justifies that the scaling method and dimensional analysis are appropriate and accurate, this confidence is enhanced by Figure 12 - comparison to Xia et. al. (2013). However, as expected, it would be incorrect to directly compare the small and medium/large vehicles when investigating other variables such as bed friction and orientation.

3.3.3 Effect of Changing Bed Friction

Vehicles could be parked on a wide variety of surfaces such as wet mud or rough asphalt, which will exhibit very different coefficients of friction. As outlined in Materials to Vary Bed Friction section (see Section 3.2.1.4), three different coefficients of bed friction were investigated: Smooth ($\mu = 0.35$), Intermediate ($\mu = 0.42$) and Rough ($\mu = 0.60$). Taking the same size vehicle and the same orientation angle for different coefficients can reveal the effect friction has on the stability:

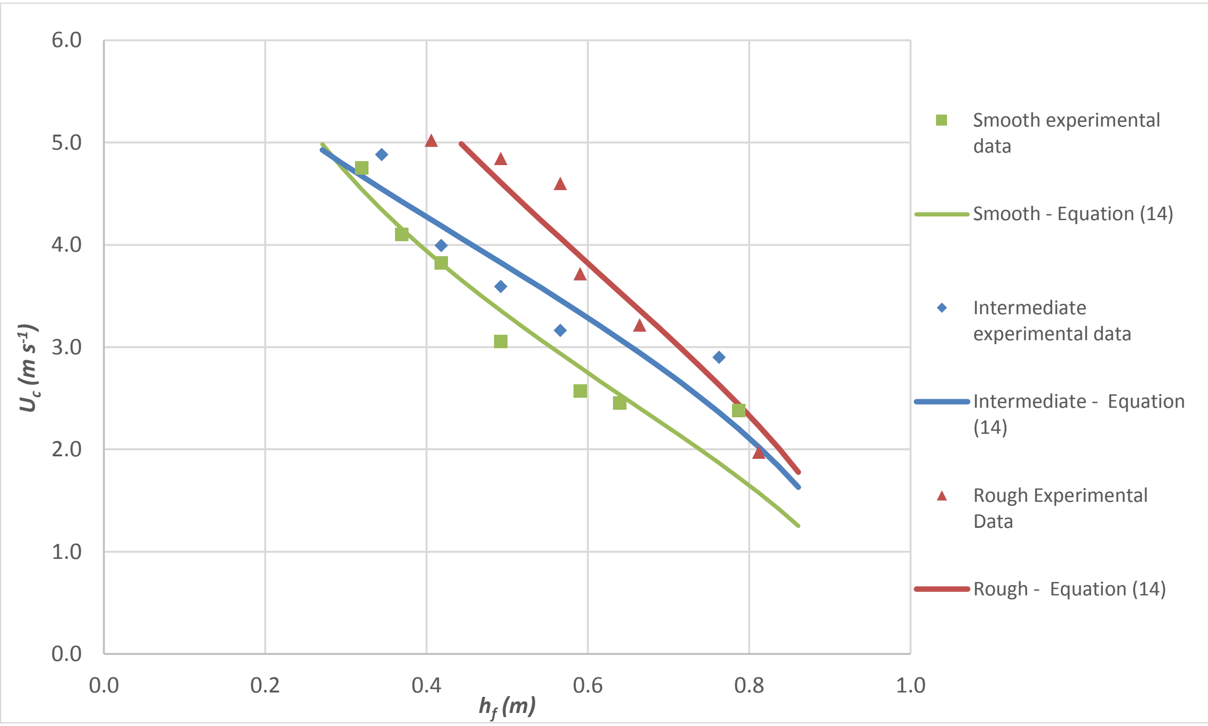

Figure 8 *Stability curves (small vehicle, 180° orientation) showing the effect of changing bed friction.*

Vehicle stability theory (see Section 3.1) identifies that U_c is proportional to $\mu^{0.5}$. Taking the "smooth" and "rough" lines and their friction coefficients yields:

$$\left(\frac{\mu_{rough}}{\mu_{smooth}}\right)^{0.5} = \left(\frac{0.601}{0.346}\right)^{0.5} = \frac{U_{c,rough}}{U_{c,smooth}} = 1.32 \qquad (18)$$

Therefore we should expect the critical velocity to be approximately 30% larger for the rough surface over the smooth surface at a given water height. This is seen in the experimental data above, where at $h_f = 0.4m$, U_c is 36% greater for the rough surface and at $h_f = 0.8m$, U_c is 51% greater. A number of other insights can be gained from Figure 8:

1. As expected from the theory, there is convergence of the stability curves of all three sets of data at high depths, and conversely divergence at low depths.
2. The intermediate surface stability curve maintains a position between the smooth and rough surfaces, although it is of a different shape. The intermediate experimental point at $U_c = 2.9\ ms^{-1}$, $h_f = 0.75m$ is the cause of this discrepancy. It would not have been unreasonable to ignore this point when optimising the free parameters α and β, however, given that there insufficient points at high depths, it was decided to include it. Section 5.2 describes the likely inaccuracies at high depths (susceptibility to unsteadiness in the flow).

Another bed friction comparison is presented in Figure 9 for the medium vehicle, in a 0° orientation.

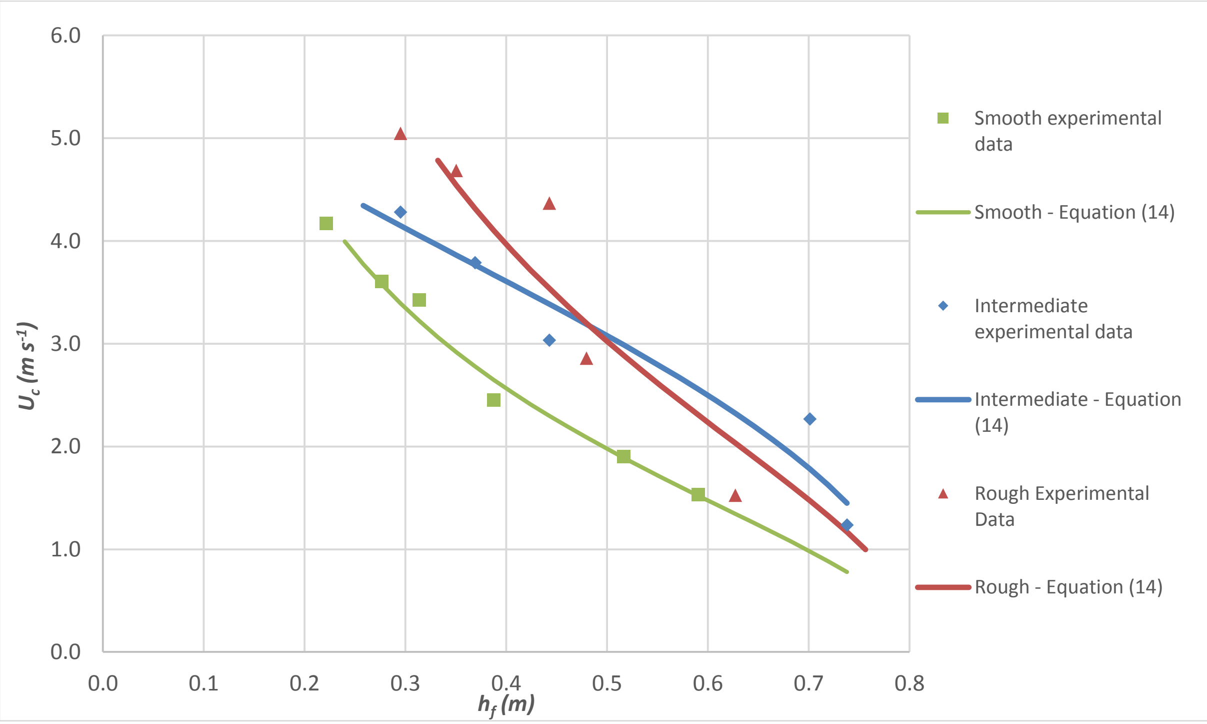

Figure 9 *Stability curves (medium vehicle, 0° orientation) showing the effect of changing bed friction.*

Figure 9 further supports the analysis presented above, this time for a different vehicle and orientation, validating the effect of bed friction on stability. Figure 9 shows fairly similar trends and results to Figure 8 (small vehicle friction comparison). The increase in U_c between the smooth and rough surfaces ranges from 60% to 50%, slightly greater than expected from the theory, but in line with the small vehicle. Again the intermediate surface roughness produces a result similar to what was witnessed for the small vehicle, where it transitions from similar to the smooth surface at high critical velocities, to being similar to the rough surface at low critical velocities. This is again attributed to experimental error (the occurrence of the near wall effect (see Section 5.1.1) at a particular velocity is likely), where there is one very obvious outlier at $h_f = 0.7m$ for the intermediate surface roughness. The point at $h_f = 0.7m$ was weighted slightly in the MATLAB regression code in an attempt to correct the curve shape, however it could not produce a reasonable curve without omitting the $h_f = 0.7m$ data point entirely, and thus the original curve is shown in Figure 9.

3.3.4 Effect of Changing Vehicle Orientation

Taking a simplistic view, changing the orientation will only change the projected area (A_d) of the vehicle normal to the flow direction. Therefore we should expect a higher drag force, and thus the critical velocity (U_c) to decrease as the projected areas is increased (e.g. the 45°, 90° and 135° orientations). The projected area for the 45° and 135° orientations is very similar to the area of the 90° orientation, and is given by:

$$A_d = a_d(h_f(b_v \sin 45 + l_v \sin 45)) \tag{19}$$

There are other factors affecting the stability that are affected by changing the orientation of the vehicle to the flow, such as:

1. The effective friction coefficient of the vehicle may change due to the directional texture of the model vehicle tyres.
2. Flow patterns around the vehicle will change and could therefore affect stability.
3. The detailed vehicle shape is different in every orientation.

Previous studies (Xia et. al. (2013)) have generally just focussed on two orientations (0° and 90°). A comparison of all five orientations is shown in Figure 10 below for the small vehicle on an intermediate surface roughness.

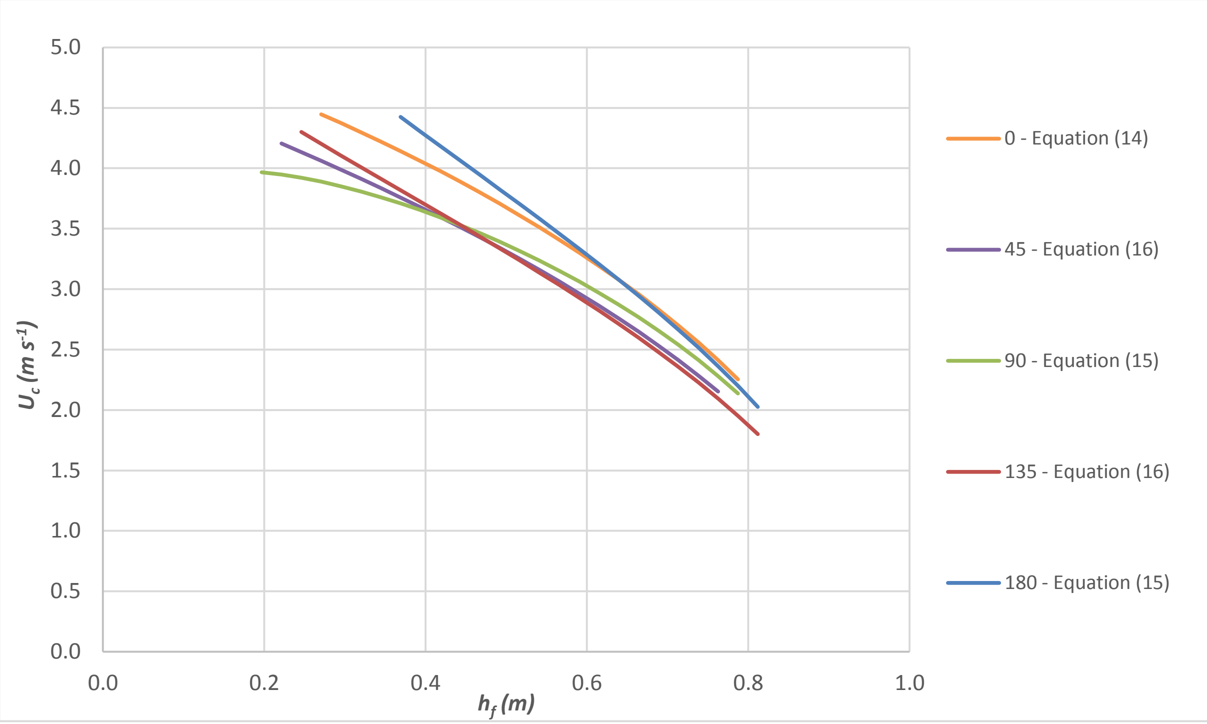

Figure 10 *Stability curves (small vehicle, intermediate surface) showing the effect of changing orientation - individual experimental data points omitted for clarity.*

Figure 10 shows that:

1. The 0° and 180° are the most stable orientations as expected, and this is in line with previous studies such as Xia et. al. (2013).
2. The 45°, 90° and 135° orientations all show very similar stability curves due to their similar projected areas. In fact, during the experiment, the 45° and 135° orientations appeared to move to a 90° orientation for a few brief moments before finally sliding, suggesting that the 90° orientation may be slightly more stable. Given this observation, it was decided to not test 45° and 135° for the other model sizes and bed surfaces.
3. The length of the model is 69mm and its width is 35mm. Given that the length of the model is roughly twice the breadth, the small difference in stability is surprisingly small between the 0°/180° and 90° orientations. From Equation (14) and Equation (15),

$$\frac{U_{c,l}}{U_{c,b}} = \left(\frac{l_v}{b_v}\right)^{0.5} \tag{20}$$

Therefore the difference in U_c between orientations for a given h_f should be approximately 40%. From the graph above, Uc for the 0°/180° orientations is approximately 20% greater than for the 90° orientation. This discrepancy is at least partly due to the model vehicle's tyre texture, which has axial grooves, producing an anisotropic friction coefficient, and would therefore increase the friction coefficient in the 0°/180° direction and increase stability in this direction.

Figure 11 shows another orientation comparison for the medium vehicle on a smooth surface.

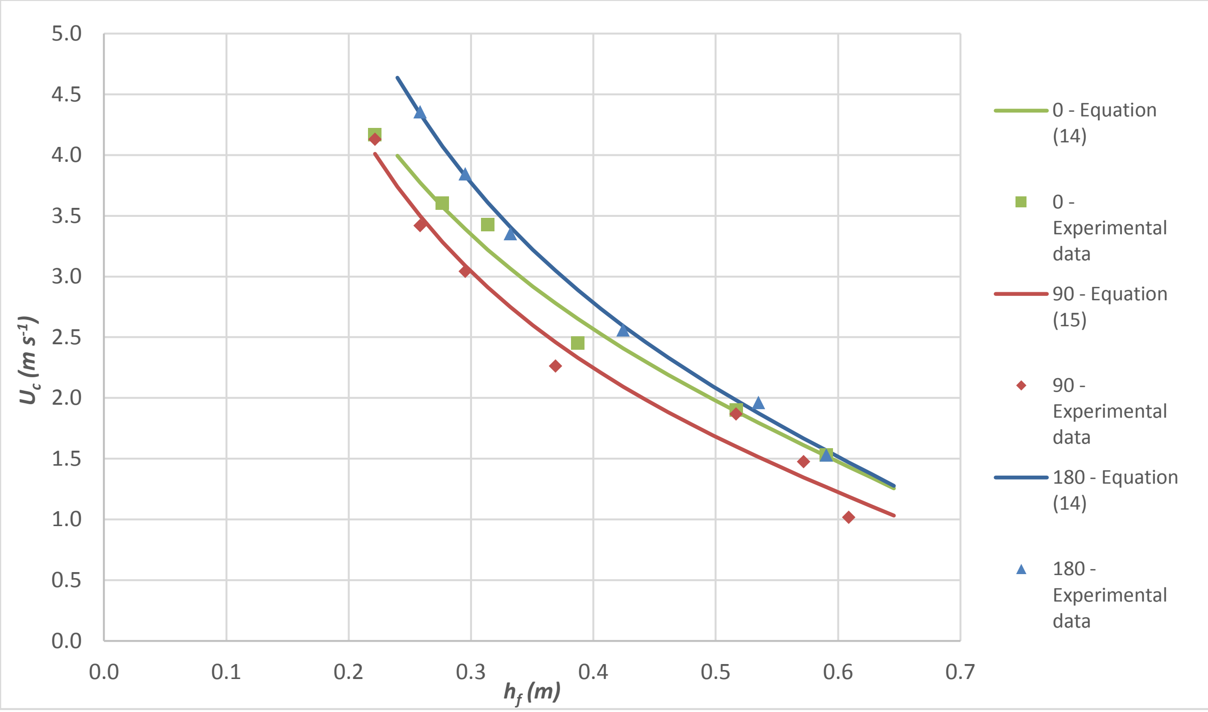

Figure 11 *Stability curves (medium vehicle, smooth surface) showing the effect of changing orientation.*

Again, the same results are expected as the small vehicle, and Figure 11 confirms this to be the case. The same explanations apply for the medium vehicle as for the small vehicle. Figure 11 also shows the difference in U_c between 0°/180° and 90° decreases as the depth increases. This is due to the vehicle approaching its floating depth, where the reaction force is reduced, and all lines must converge to the stationary floating depth, h_k, on the x-axis.

3.3.5 Comparison with Previous Studies

3.3.5.1 Xia et. al. (2013)

As mentioned in the literature review (see Section 1.3), many previous studies have been carried out on the stability of vehicles. Xia et. al. (2013) is of particular interest since it is very recent and uses similar methodology, models and also considers two characteristic orientations (0°/180° and 90°). The results were plotted alongside Xia et. al. (2013) by using

DataFig software, which was supplied by Dr Liang. The DataFig software converts an image of a graph into raw data (by manually clicking on the data points in the program), which can then be plotted alongside the data obtained in this study.

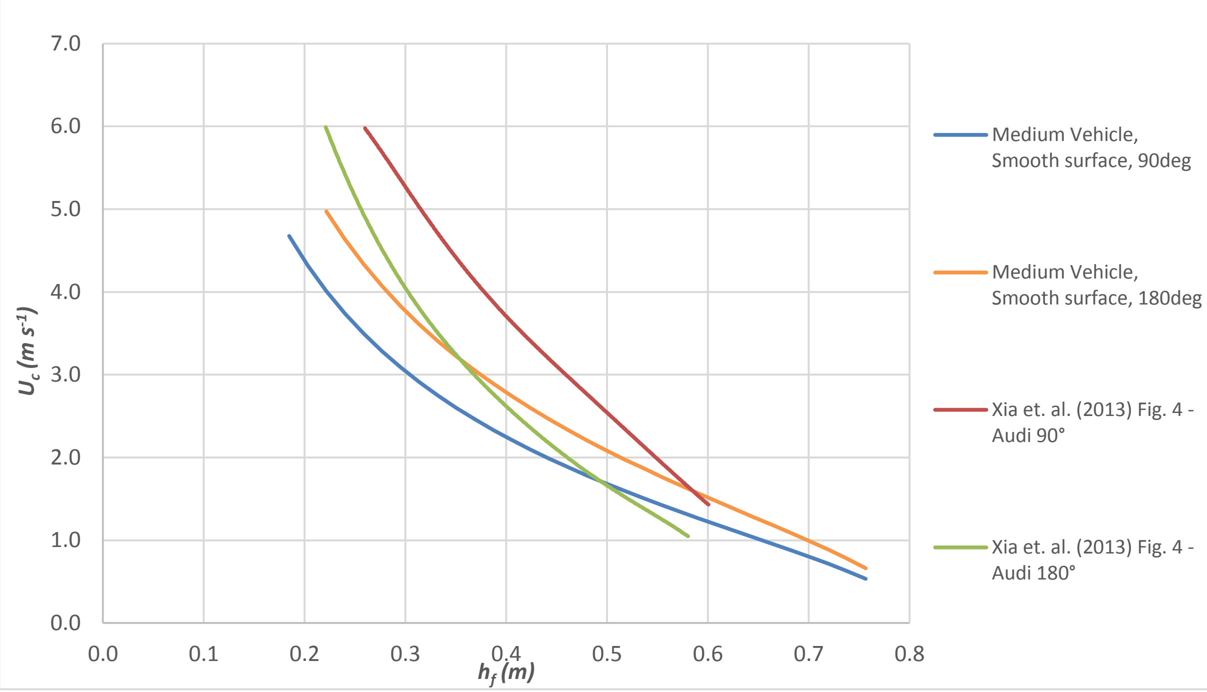

Figure 12 *Stability curves (medium vehicle, smooth surface, 90° and 180° orientations) showing a comparison to Xia et. al. (2013).*

There is reasonable correlation to the results of Xia et. al. (2013), including a similar difference between 90° and 180° orientations. There is however a discrepancy between the critical velocity, especially at high velocities, which can be explained by considering the differences between the two experiments:

1. Model vehicles: Xia tested two models (a model Audi and model Honda), neither of which have a similar shape to either of the models used in this study. The medium vehicle was thought to have the greatest shape similarity to the Audi.
2. Xia quotes a friction coefficient of “between 0.25 and 0.75”, compared to 0.35 for the smooth surface shown in the figure above. Therefore it is likely that Xia used a larger friction coefficient, resulting in the more stable curve.

Xia’s study doesn’t consider changing the bed friction, so it is difficult to validate that part of the experiment against Xia et. al. (2013).

3.3.5.2 Keller and Mitsch (1993)

Keller and Mitsch produced a purely theoretical study on the stability of vehicles in floodways. They did this by calculating a detailed force equilibrium for sliding at incremental water depths. Their results are shown below:

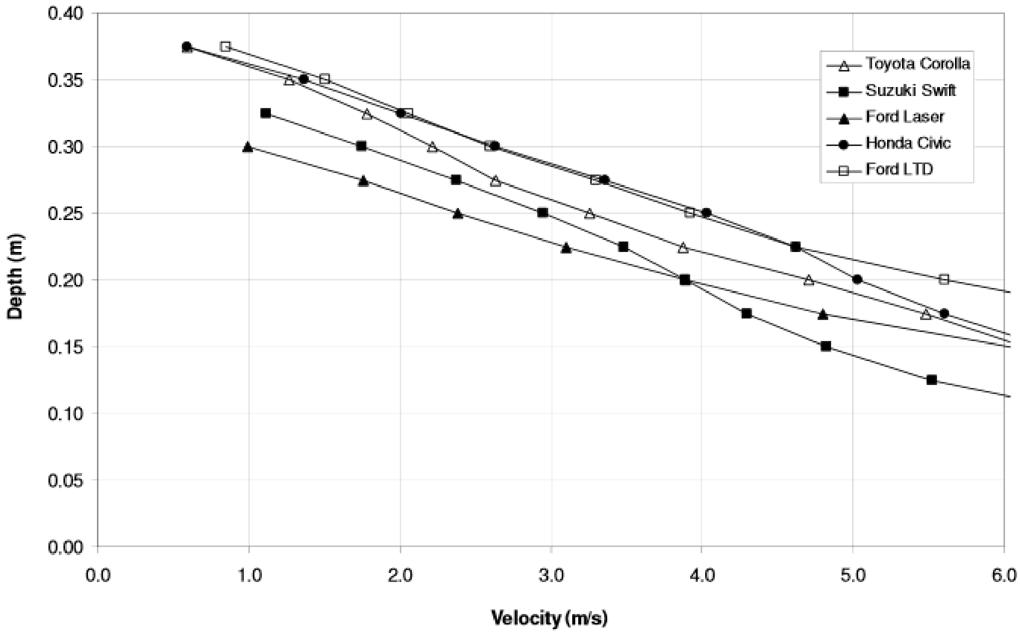

Figure 13 *Keller and Mitsch's stability curves for various vehicles - note the reversed axes. Figure taken from Shand et. al. (2011).*

These results have been replotted (using DataFig) to enable comparison to this study:

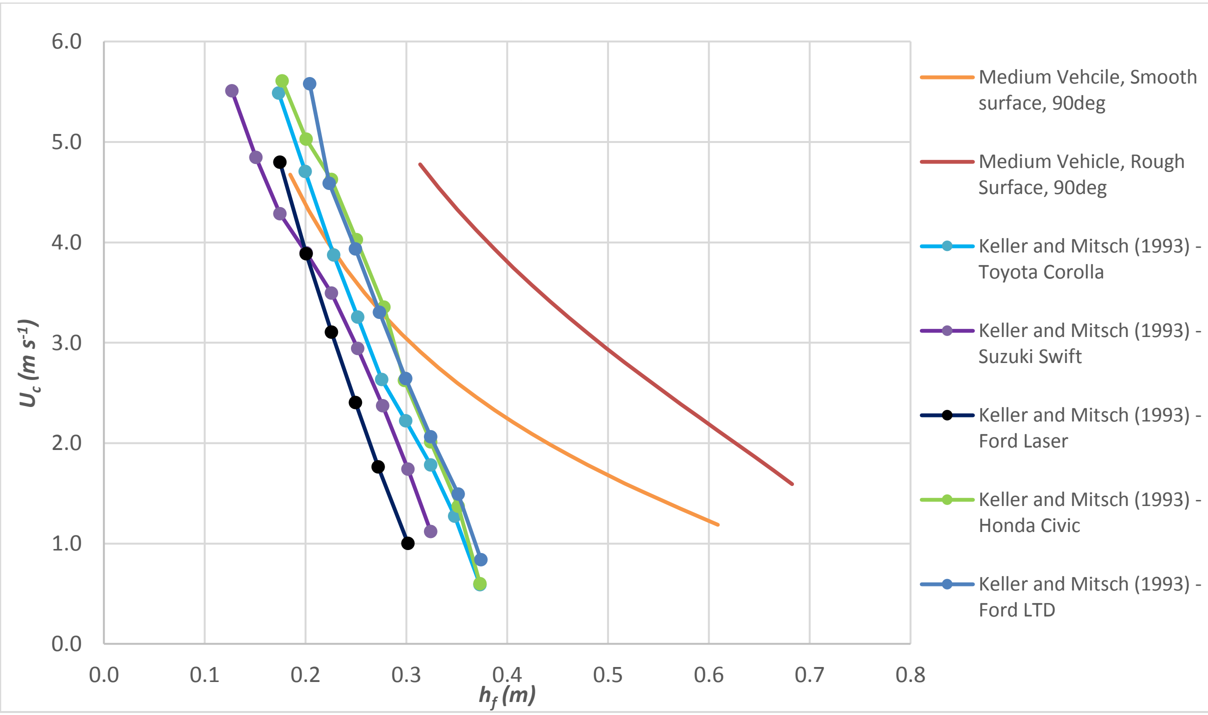

Figure 14 *Stability curves (medium vehicle, smooth/rough surfaces, 90° orientation) showing a comparison to the theoretical results Keller and Mitsch (1993), note the reversed axes to Figure 13.*

Since Keller and Mitsch only considered flows at 90°, and assumed a coefficient of friction of 0.3, the medium vehicle with smooth surface and 90° orientation data set is the most appropriate for comparison. Also included on Figure 14 is the equivalent data set but with a rough surface. Keller Mitsch's approach has produced significant differences in the results:

1. This study suggests vehicles are significantly more stable at higher depths
2. The shape of Keller and Mitch's curves completely contradict both this study and Xia et. al. (2013).

Keller and Mitsch calculated the centre of buoyancy and weight distribution at incremental depths (from detailed manufacturer specifications for real cars), in order to find the reaction forces. This is the root of the discrepancy, where real vehicles (as used in Keller and Mitsch) are likely to have a relatively much lower ground clearance than the model vehicles, which would result in a much lower floating height (h_k) (as seen above). Other experimental scaled model studies have produced much higher estimated floating heights than Keller and Mitsch, for example Bonham and Hattersley (1967), (although an old experiment its recorded floating heights are still valid) assumed a floating height of 0.57m. Xia et. al. (2013) also recorded floating heights of 0.45m to 0.67m. Therefore Keller and Mitsch's assumed floating heights (of approximately 0.35m) are significantly different. However, given that Keller and Mitsch used manufacturer's data for real cars, it may be a problem for all scaled experimental studies that they overestimate vehicle stability at high depths, which is worthy of more investigation.

Figure 14 also shows a fundamentally different curve shape between the studies, with Keller and Mitsch clearly adopting a very conservative theoretical approach at higher depths, that doesn't compare well to experimental studies.

3.3.6 Suggested Vehicle Stability Criteria

Floodway flow may be incident on a vehicle in any orientation or bed roughness type. A sensible approach is therefore to take the most conservative stability curve – medium car, smooth surface, 90° orientation. This will produce a lower bound, below which the floodway conditions will pose a low hazard to all vehicles. An upper bound can be produced by taking the least conservative stability curve (small vehicle, rough surface, 180° orientation) above which all vehicles will be at severe risk of instability.

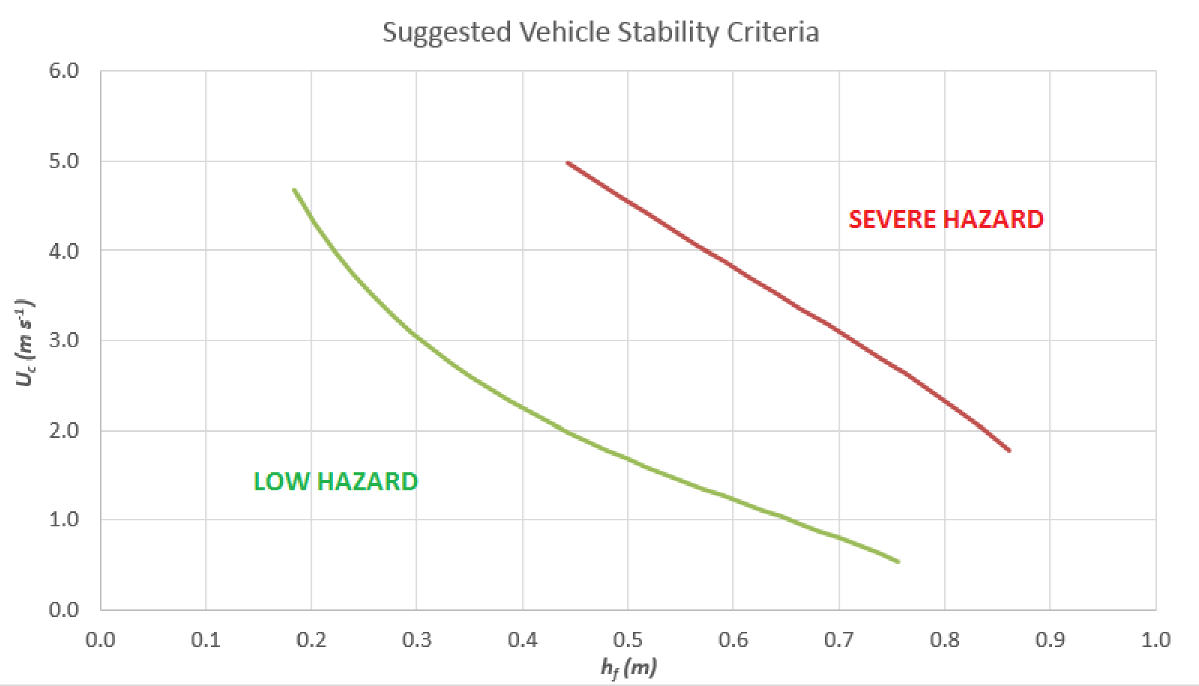

Figure 15 *Suggested vehicle stability criteria for floodways*

4 Human Stability in Steady Flow

4.1 Human Stability Theory: Force Analysis and Formula Derivation

In this section, a theoretical analysis of the forces acting on a human in a floodway is carried out, in a similar way to the analysis carried out for the vehicle (see Section 3.1). This analysis is based on Xia et. al. (2014), although a few changes have been made. There are a few key differences in the analysis for a human body to that of the vehicle:

1. There are two instability mechanisms (toppling and sliding), which will need to be considered separately.
2. Ergonomic data for an average human (for example relative volume of body segments) is considered when calculating buoyancy forces.
3. Floating is not considered as an instability mechanism due to the fact that the average human is denser than water.

The forces acting on a human body in a floodway are defined as shown in Figure 16:

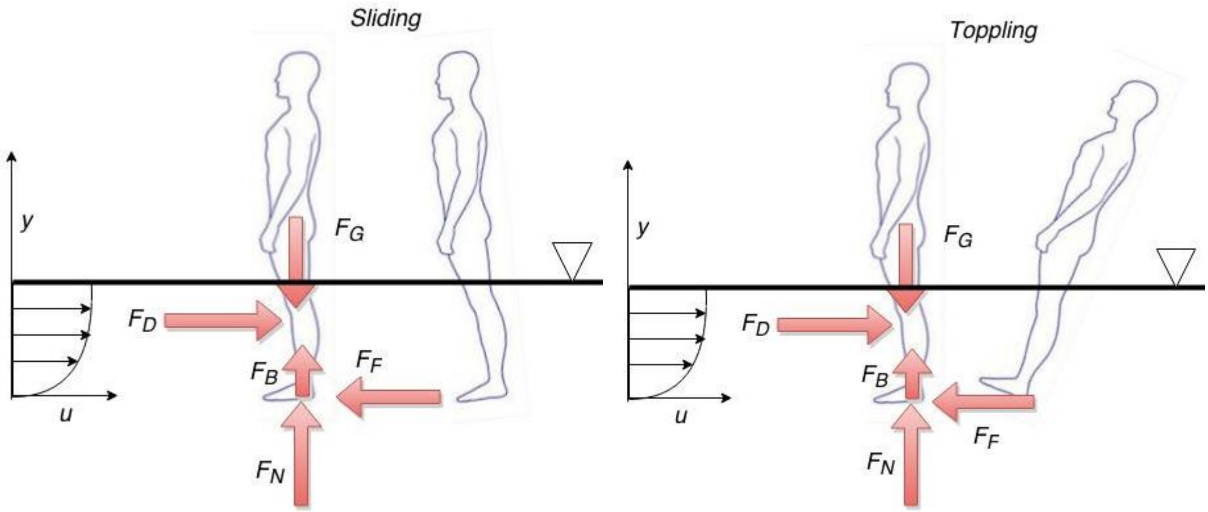

Figure 16 *Diagram showing the forces acting on a human body in a floodway for sliding (left) and toppling (right) instability mechanisms.*

There are five forces acting on the human: buoyancy force (F_B), drag force (F_D), friction force (F_F), weight (F_G) and normal reaction force (F_N). Definitions for the parameters in the following analysis are given in the main text.

4.1.1 Buoyancy Force

The buoyancy force acting on a body is given by $F_b = \rho_w g V_b$ where V_b is the volume of water displaced by the human. Since the human body is an irregular shape, V_b will need to be found through relationships relating the relative sizes of body segments (see Figure 17 for an example of relevant anthropometric data). The results obtained by Drillis et. al. (1964) are appropriate and will be used in this analysis. This is different from the values used by Xia et. al. (2014), who used relationships relating to the average Chinese adult, whereas Drillis published results for American subjects. V_b can then be expressed as:

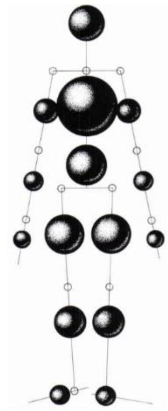

Figure 17 *Taken from Drillis et. al. (1964)*

$$\frac{V_b}{V_p} = a_1 \left(\frac{h_f}{h_p}\right)^2 + b_1 \frac{h_f}{h_p} \tag{21}$$

Where V_p is the total human volume, h_p is the total human height, h_f the height of the flow and a_1 and b_1 are the coefficients published by Drillis et. al. (1964) and are given as $a_1 = 0.737$ and $b_1 = 0.263$. To avoid having to find the total human volume, V_p can be related to m_p by a relationship published by Guo and Wang (1995):

$$v_p = a_2 m_p + b_2 \tag{22}$$

Guo and Wang determined $a_2 = 0.001015\ m^3kg^{-1}$ and $b_2 = -0.004927\ m^3$, which are also the values used by Xia et. al. (2014). Substituting Equation (21) and Equation (22) into the equation for F_b yields (the only unknown is h_f):

$$F_b = g\rho_w (a_1 \left(\frac{h_f}{h_p}\right)^2 + b_1 \frac{h_f}{h_p})(a_2 m_p + b_2) \tag{23}$$

4.1.2 Drag Force

The drag force is given by the familiar equation:

$$F_D = \frac{1}{2} C_d \rho_w A_d u^2 \tag{24}$$

Where C_d represents the drag coefficient, u is the representative near bed velocity and A_d is the projected area normal to the flow. To find A_d we can multiply the depth of incoming flow by the average body width exposed (b_p), giving $A_d = b_p h_f \alpha_d$. To account for the effect of clothes, coefficient a_d is used. The average body width exposed will vary depending on the orientation of the human relative to the flow. A numerical value for C_d does not need to be calculated because it will be included in the parameter calibration to the experimental data.

4.1.3 Frictional Force

The static frictional force can simply be given by the coulomb model for friction, $F_F = \mu F_N$, where μ is the coefficient of friction between the shoes and floor and F_N is the normal reaction force.

$$F_f = \mu F_n = \mu(m_p g - F_b) = \mu g(m_p - \rho_w(a_1\left(\frac{h_f}{h_p}\right)^2 + b_1\frac{h_f}{h_p})(a_2 m_p + b_2)) \tag{25}$$

Now that the forces have been defined, force balances can be used to determine the point of instability for both sliding and toppling. Sliding instability will occur when the drag force just exceeds the frictional force: $F_D = F_F$. Toppling instability will occur when the body pivots about the heel (as seen in Figure 16 above), which can be determined from a moment balance about the heel of the human.

4.1.4 Formula Derivation for Sliding Instability

Following the same process as for the sliding vehicle (see Section 3.1.4), the formula relating critical velocity to incoming flow height can be shown to be:

$$U_c = \alpha\left(\frac{h_f}{h_p}\right)^{\beta}\sqrt{\frac{1}{b_p}\left[\frac{m_p}{\rho_f h_p h_f} - (a_1\frac{h_f}{h_p} + b_1)\frac{(a_2 m_p + b_2)}{h_p^2}\right]} \tag{26}$$

Where,

$$\alpha = \frac{\sqrt{2\mu g/(C_d a_d)}}{(1+\beta)(a_b)^{\beta})} \tag{27}$$

This is slightly different to the formula derived by Xia et. al. (2014), since Xia was only testing the 0° case, the normal projected area would not change due to changing orientation. In this study the effect of changing posture (and therefore changing normal projected area) was considered and therefore the equation will have to be modified to account for the different projected areas of each orientation. Three orientations were considered (0°, 45° and 90°) and this will result in three equations for sliding, three more equations for toppling and therefore six in total. Although these changes will not affect the shape of the curve dramatically, it doesn't allow easy direct comparison of the values of α and β obtained in Xia et. al. (2014).

4.1.5 Formula Derivation for Toppling Instability

The drag force and effective weight both create moments about the heel. If L_D is the lever arm of the drag force and L_G the lever arm of the effective weight, then taking moments about the heel gives:

$$F_D L_D - F_G L_G = 0 \tag{28}$$

Taking L_D and L_G as fractions of the flow height and human height respectively ($L_D = a_h h_f$ and $L_G = a_g h_p$), and substitution of the force equations into Equation (28) gives:

$$U_c = \alpha \left(\frac{h_f}{h_p}\right)^{\beta} \sqrt{\frac{h_p}{b_p}\left[\frac{m_p}{\rho_f h_f^2} - \left(\frac{a_1}{h_p^2} + \frac{b_1}{h_f h_p}\right)(a_2 m_p + b_2)\right]} \tag{29}$$

Where,

$$\alpha = \sqrt{\frac{2 g a_g}{C_d a_d a_h a_b^{2\beta} (1+\beta)^2}} \tag{30}$$

Again this gives a slightly different formula to Xia since the parameter b_p needs to be included outside of α for clarity. Linear regression will be used to fit the experimental data to the above curve shapes, giving numerical values for α and β.

4.2 Apparatus and Experimental Techniques

4.2.1 Apparatus

The same wave flume and measurement apparatus were used for the human stability investigation as the vehicle stability investigation (see Section 3.2.1). A sheet of 1200 grade sandpaper was assessed (using the method described in the Materials to Vary Bed Friction section (see Section 3.2.1.4)) to have a friction coefficient of 0.51. Takahashi et. al. (1992) conducted tests on a range of shoes and surfaces and determined that μ could vary between 0.2 and 1.5, and Xia et. al. (2013) covered the water flume in grit in order to achieve a friction coefficient of 0.5. It is therefore assumed that the friction coefficient of 0.51 is appropriate, and will therefore not be varied throughout the experiments.

4.2.1.1 Models

Three different sized models were used, the large and small models can be seen in Figure 18 (with additional mass added). The medium sized model was not used because the joints were too loose to maintain any form of standing posture. From the dimensional analysis (see Section 2.2), extra mass was required to be added to each model. The aim was to add mass in such a way that the shape similarity between models would not be adversely affected too greatly, and to maintain a centre of gravity similar to that of a real human. The centre of gravity of the models was found using the traditional method of hanging the models from different places and using a plumb line to triangulate the centre of gravity (seen on the models lower torso in Figure 18). The models were chosen for their apparent shape similarity, however some features (such as feet) do not conform to the scaling ratio.

Figure 18 *Small and Large models with centres of gravity marked on the lower torso.*

Table 6 *Measured parameters of the three models, with scale factors calculated.*

	Real Human	**Small**	**Medium**	**Large**
Height (cm)	170	14	20	30
Length Scale	1	12.1	8.5	5.7
Velocity Scale	1	3.5	2.9	2.4
Mass before (g)	-	22.1	49.6	145.1
Mass required (g)	60000	34.2	97.7	329.7

4.2.2 Experimental Procedure

All results were obtained using the apparatus as described in the Apparatus sections (see Section 3.2.1 and Section 4.2.1). As, with for the vehicle stability study, it was necessary to validate the scaling of the three model sizes, requiring results for the small and large model. A major aim of the project was to investigate the effect of posture on human stability in floodways and so six systematic postures were considered along with various “custom postures”, see Table 7 (next page).

Table 7 *Summary of results obtained for human model experiments*

		Orientation to flow		
		0°	45°	90°
Large Model	Narrow Stance	✓	✓	✓
	Wide Stance	✓	✓	✓
Small Model	Narrow Stance	✓		

The narrow stance is 5 cm wide from feet centre to centre (roughly shoulder width), whereas the wide stance is 10 cm from feet centre to centre. These results sets typically had many more readings than those for the vehicles (approximately 11 readings per set) because the flow depth was much greater. The act of taking the readings was exactly the same as for the vehicle stability experiment and will not be repeated here (see Section 3.2.2).

4.3 Results and Discussion

The results section is split up into the following sections:

1 Parameter calibration and investigating the different size models to confirm the scaling is correct.
2 Investigating the effect of posture on stability.
3 Comparison of the results against similar previous studies.

4.3.1 Parameter Calibration

MATLAB was again used to perform linear regression and fit Equation (26) and Equation (29) to the experimental data, as explained previously for the vehicle stability analysis (see Section 3.3.1). The following parameters were used in the equations in order to find α and β:

Table 8 *Values of the parameters used in Equation (26) and Equation (29).*

Parameter	Name	Value	Units
a_1	Coefficient for buoyancy force determination	0.737	-
b_1	Coefficient for buoyancy force determination	0.263	-
a_2	Coefficient for relationship between volume and mass	0.00102	$m^3\ kg^{-1}$
b_2	Coefficient for relationship between volume and mass	-0.00493	m_3
m_p	Average human mass	60.0	kg
h_p	Average human height	1.70	m
P_w	Water density	1000	$kg\ m^{-3}$
b_p (0°)	Average body width exposed normal to flow (0°)	0.40	m
b_p (45°)	Average body width exposed normal to flow (45°)	0.45	m
b_p (90°)	Average body width exposed normal to flow (90°)	0.30	m

The values for b_p were calculated assuming a human thigh has dimensions 0.2m wide and 0.3m deep. An example curve fitting plot using MATLAB is shown in Figure 19:

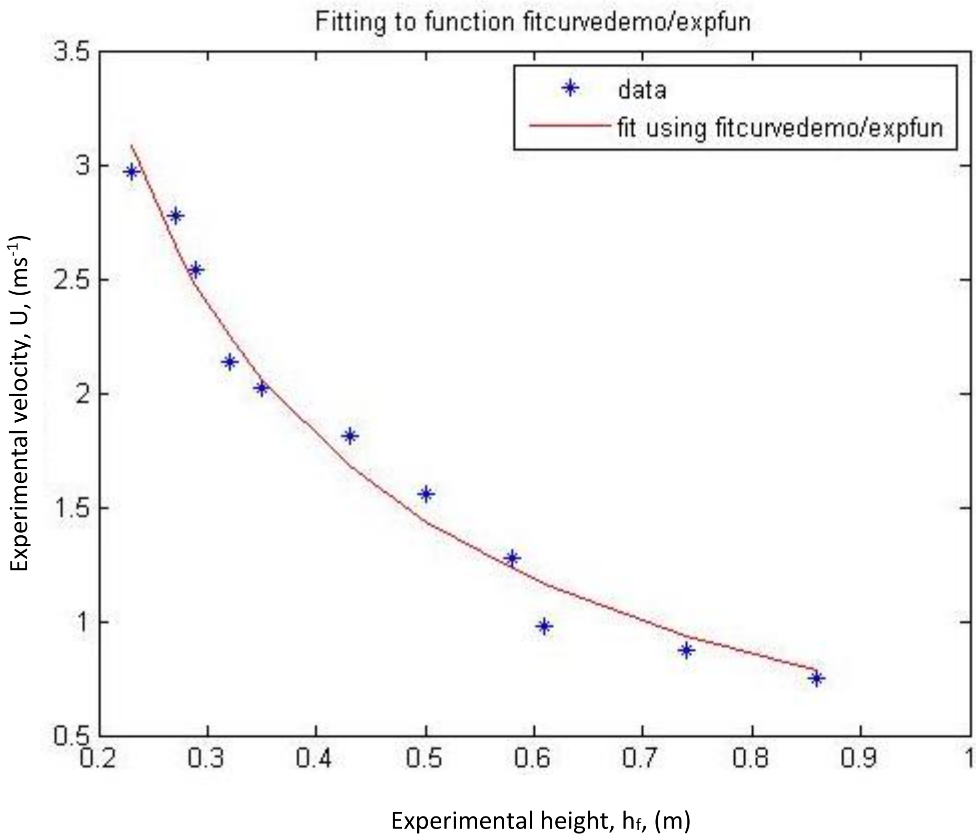

Figure 19 *Example MATLAB curve fitting for the narrow, 45°, toppling case.*

After performing the MATLAB analysis for all sets of results the following parameters were obtained:

Table 9 *Calibrated free parameters in Equation (26) and Equation (29).*

			0°		45°		90°	
			α ($m^{0.5}s^{-1}$)	**β (-)**	**α ($m^{0.5}s^{-1}$)**	**β (-)**	**α ($m^{0.5}s^{-1}$)**	**β (-)**
Large Model	**Sliding**	**Narrow**					0.72	-0.62
		Wide			0.33	-0.90	0.18	-1.53
	Toppling	**Narrow**	0.51	0.14	0.56	0.08	0.69	0.09
		Wide	0.41	-0.11	0.62	0.13	0.63	-0.04
Small Model		**Sliding**	1.35	-0.49				
		Toppling	0.23	-0.21				

It is worth noting that these parameters are different to the ones obtained by Xia et. al. (2014), due to the modified equations being used. The parameters above are used to plot the stability curves shown on the figures in the following results sections.

4.3.2 Human Size Comparison

To verify the scaling method used was accurate, the large and small models can be compared after the depth and velocity measurements have been scaled.

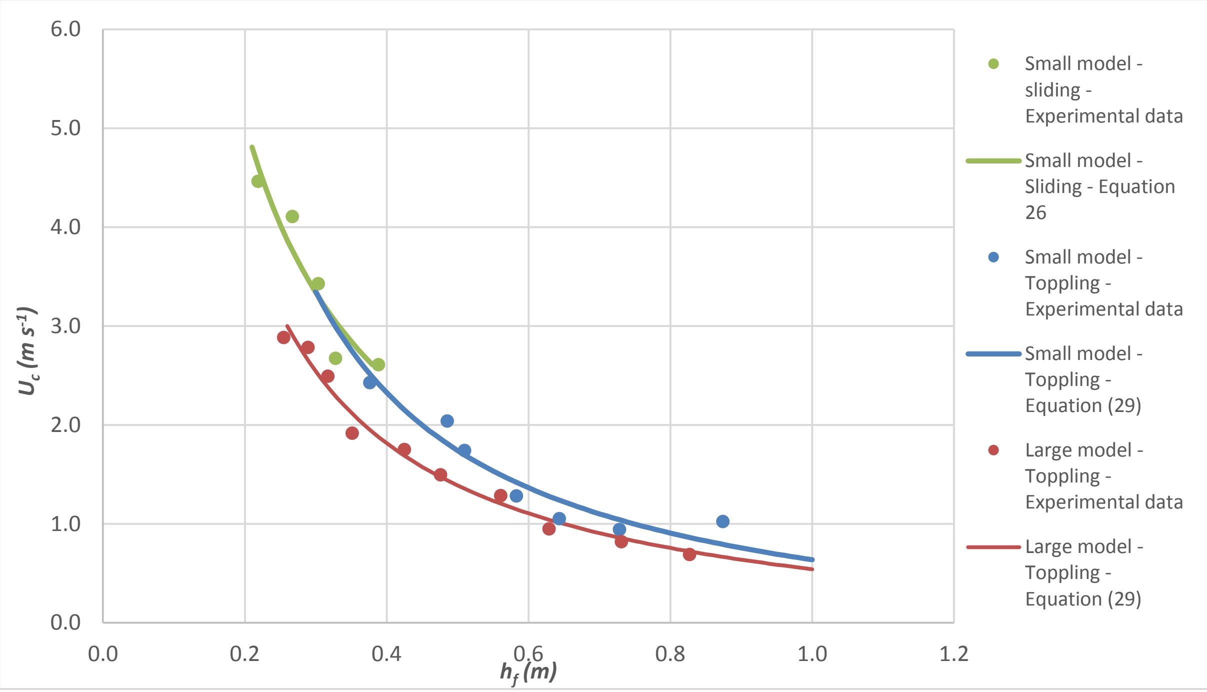

Figure 20 *Stability curves (small and large models, 0° orientation) validating the scaling procedure.*

There are small experimental differences in the large and small model tests. Firstly, the water flume is working close to the limit of its capacity for the large model, producing more unsteady flow effects and therefore they will not completely settle down before the working area of the flume. This will result in premature failure of the large model: consistent with Figure 20. Secondly, not all of the model's dimensions scale with the geometric ratio. However, the overall the shape and magnitude of the curves are similar enough (within the inaccuracies outlined) to justify the scaling method. This enables the subsequent tests to be performed with only the larger model, with confidence that it can be scaled up to real human size successfully. The larger model was chosen because it was easier to fix the posture precisely.

Figure 20 shows that the relative difference in critical velocity between small and large models at a given depth increases for lower depths (maximum difference in U_c is 30%). This is likely to be due to the small model beginning to transition sliding instability at lower depths, whereas the larger model did not shown transition to sliding to the same degree.

4.3.3 Posture Investigation

In order to investigate the effects of posture on the stability of a human body it was first necessary to simplify the very large number of possible human postures. Two aspects of posture were deemed to be most important for stability: stance width and orientation to the flow direction. Therefore, a systematic approach was used whereby two widths of stance (narrow and wide) and three orientations (0°, 45° and 90°) were considered, (see Section 4.2.2 for more detail). Posture covers a broad range of aspects affecting human stability such as body lean angle, feet angles, bends in joints etc. It would be very time consuming to measure the change in stability from each separately and therefore for the second part of the posture investigation focussed on creating the most stable postures.

4.3.3.1 Orientation and Stance Width Investigation

Considering only the effect of stance width to begin with, Figure 23 was produced, showing the toppling stability curves for both stances in two orientations. A wider stance will have the following effects:

1. Reduction in the height of the centre of gravity above the bed surface,
2. Increase in the frontal projected area normal to the flow direction,
3. Increase in the effective width of the base (not for the 0° orientation),

The large model has a leg length of 13 cm and, using simple geometry, the height of the centre of gravity changed from 12.75 cm to 12 cm from changing the stance width from narrow to wide. This represents an increase in effective projected area of at least 12%. Equation (29) shows that U_c is more dependent on L_G than A_D and therefore it is expected that the positive stabilising effect of lowering the centre of gravity will prevail over the destabilising effect of the increase in projected area.

This is justified by Figure 23, which shows the wide stance to be slightly more stable (from 0 to 20% increase in U_c) for the 0° orientation, with the stability difference increasing with increasing velocity.

For the 90° orientation, a wider stance should increase toppling stability significantly. This is because of the greater base width. Only a modest increase in stability was noted from Figure 23. This is because the model was observed to topple about its minor axis (perpendicular to flow direction), for both stance widths. Turbulent or unsteady effects can create transverse forces (perpendicular to flow direction) across the model, resulting in the toppling direction observed.

Sliding stability is not affected by stance width (as expected), as seen in Figure 21 where both narrow 90° and wide 90° have very similar results. This should be the case since neither reaction force, feet area or friction coefficient are changed by stance width.

It is worth noting that this may not translate to a real human scenario, where a wider stance width (for the 90° orientation) is likely to be the result of an attempt to "anchor" the back foot to increase friction coefficient or provide a horizontal force component. This is just one of the numerous examples where the intuitively best posture for a real human to resist the flow cannot be investigated accurately with a rigid scale model – discussed more in the Experimental Accuracy and Sources of Error section (see Section 5).

The effect of changing orientation angle is to:

1. Change projected area normal to the flow.
2. Change base width in the direction of flow to change susceptibility to the toppling failure mechanism.

Firstly, according to Equation (29), the following relationship is apparent:

$$U_c \;\alpha\; \sqrt{\frac{1}{b_p}} \qquad (31)$$

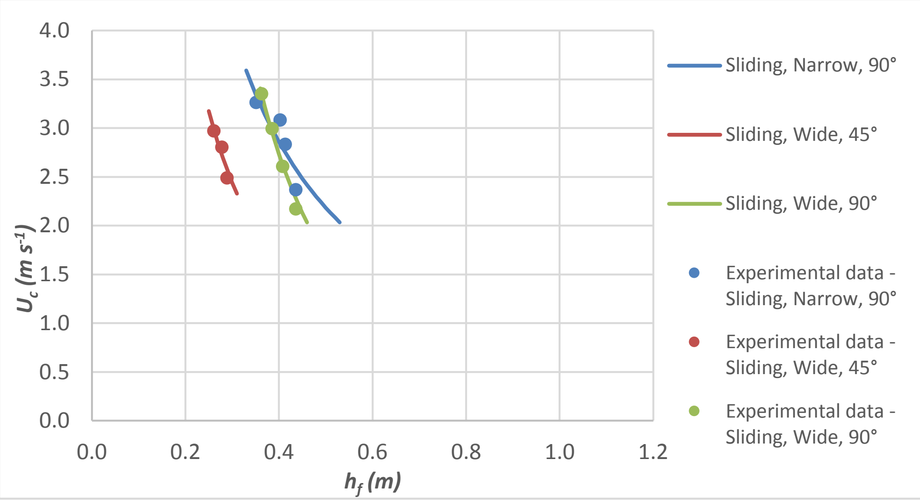

Figure 21 *Stability curves for the sliding mechanism only.*

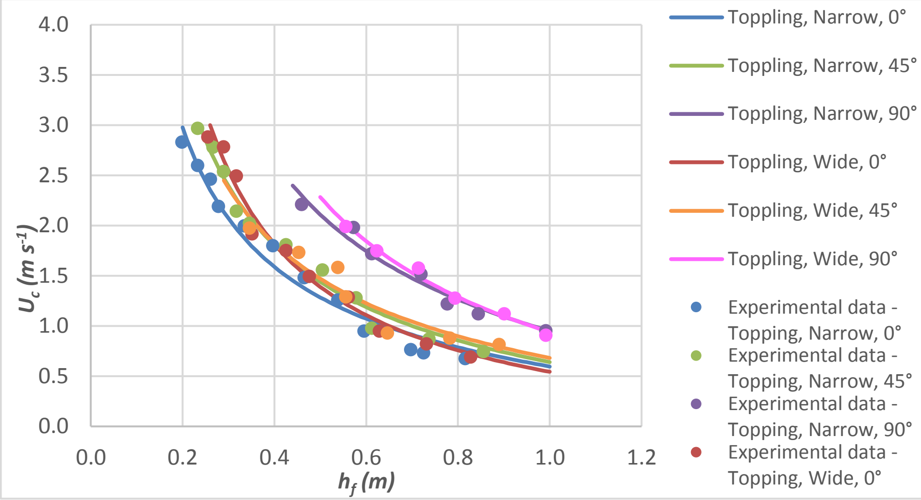

Figure 22 *Stability curves for the toppling mechanism only.*

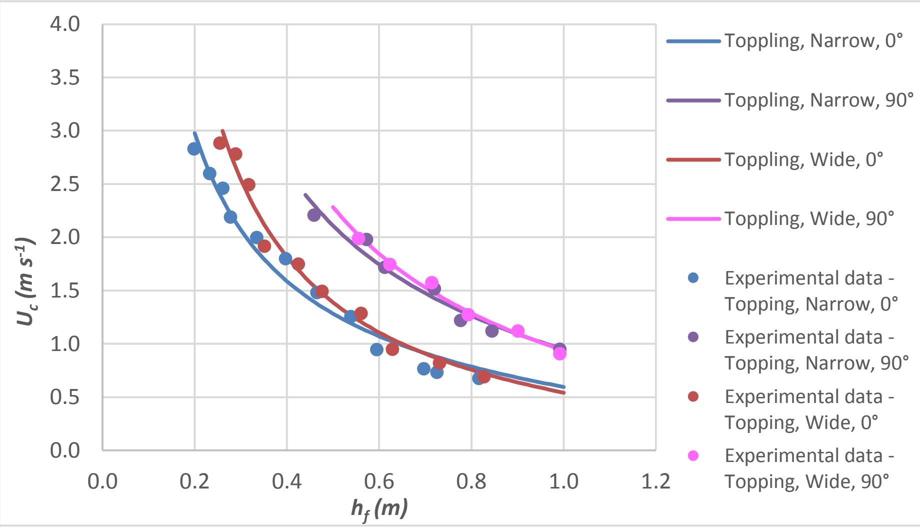

Figure 23 *Stability curves showing the effect of changing stance width*

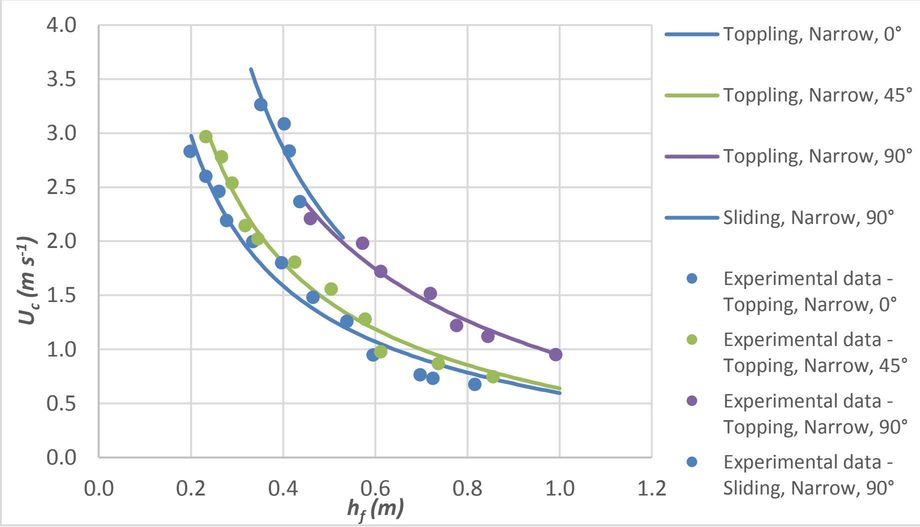

Figure 24 *Stability curves showing the effect of changing orientation.*

Equation (31) shows that changing the orientation from 90° to 0° should result in a 13% reduction in critical velocity at a iven depth:

$$\frac{U_{c,0}}{U_{c,90}} = \sqrt{\frac{b_{p,90}}{b_{p,0}}} = 0.866 \tag{32}$$

The actual difference in U_c, from Figure 24 above, varies from approximately 0.57 at low depths to 0.67 at higher depths, a much larger difference than the theory predicted for changing projected area. Causes of this discrepancy are:

1. Increasing base width in the flow direction resulting in increased toppling resistance and greater stability. This is the cause of the vast majority of the discrepancy noted above.
2. The values for b_p (average body width in flow) are best guess estimates from the available leg measurements and difficult to judge since average body width in the flow will change with flow depth. There could well be up to 20% error in the value of b_p. This error would not dramatically change the curve shape however.

For the case of 90° orientation, it may not be fully correct to assume that the area the drag force acts on is just the frontal projected area, since there will also be some water impacting the back leg and creating drag force.

For the 45° orientation, Figure 24 shows that it is marginally but consistently more stable with the critical velocity increasing by approximately 10% for a given depth. The increase in projected area for the 45° case would result in a larger drag force acting on the model. However, in order to topple the model, the moment must act about the minor axis (shown on Figure 25 below), with only a *sin45°* component of the drag force acting in the appropriate direction. The two combined effects lead to the modest increase in stability seen.

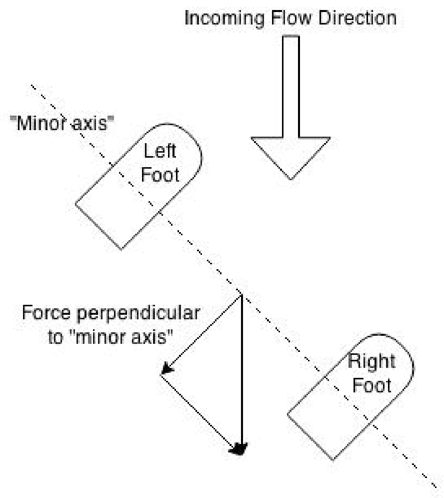

Figure 25 *Schematic plan view diagram showing drag forces acting on the model in 45° orientation*

It is also worth noting the flow criteria required for the sliding mechanism to dominate, Figure 21 suggests flows with velocity over 2.5 ms^{-1} may induce sliding. Shand (2011) and Xia et. al. (2014) both suggest 3 ms^{-1} is required for sliding to dominate. The experiment proved that it is very difficult to judge the failure mechanism accurately and objectively. It is possible for both mechanisms to combine, for example slight rocking of the model will reduce feet contact area and precipitate sliding failure. This will lead to incorrect reporting of failure mechanism, which explains why there is an overlap of the occurrence of sliding and toppling when comparing Figure 21 and Figure 22. As a general rule, any floodway with a velocity over 2.5 ms^{-1} will be at risk causing human sliding failure.

4.3.3.2 Other Postures

In an effort to capture more subtle effects of changing posture than stance width and orientation, several custom postures were tested, an example of which can be seen below in Figure 26. Based on intuition and trial and error, attempts were made to maximise stability. The subtle changes in posture that were considered were forward lean, bent front knee and back foot perpendicular to minor axis. These “custom postures” were tested in the 0° orientation.

Figure 26 *Example "custom posture". (Front view (Left) and Side View (Right))*

The custom posture shown in Figure 26 was found to be the most stable, the experimental results are provided in Figure 27, alongside results from the orientation and stance width investigation. The toppling mechanism equation, along with 0° orientation, were used to calibrate the free parameters, which were found to be $\alpha = 0.6296$ $m^{0.5}s^{-1}$, and $\beta = 0.3079$. Figure 27 shows the custom posture was more stable at higher depths than the 0° orientation. Of course, this is due to the increased toppling resistance from having a larger base in the flow direction. Given the modest stability increase, it is reasonable to suggest orientation (and therefore effective projected area) is the most important aspect of the combined posture effects.

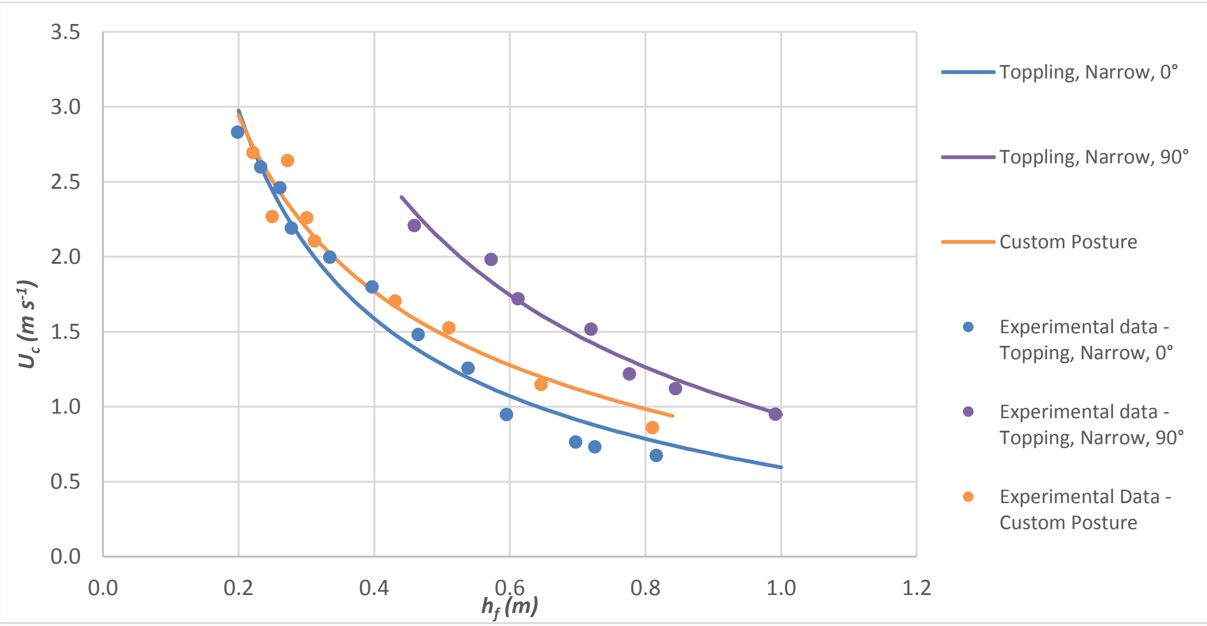

Figure 27 *Stability curve for the custom posture. 0° and 90°, narrow stance stability curves are included for reference.*

4.3.4 Comparison with Previous Studies

As outlined in the Literature Review (see Section 1.3), Xia et. al. (2014) is a similar recent scale model study of human stability and can be directly compared to this experiment. Xia et. al. (2014) only investigated 0° cases, and therefore both narrow and wide 0° cases have been plotted against Xia's data in Figure 28. The line labelled: "Xia et. al. – Equation (13)" is a stability threshold suitable for children, which was suggested by Xia et. al. (2014) and can be found in Figure 7 of Xia et. al. (2014). The raw data was extracted from the published results using DataFig software, which has been described previously for the vehicle stability experiment (see Section 3.3.5).

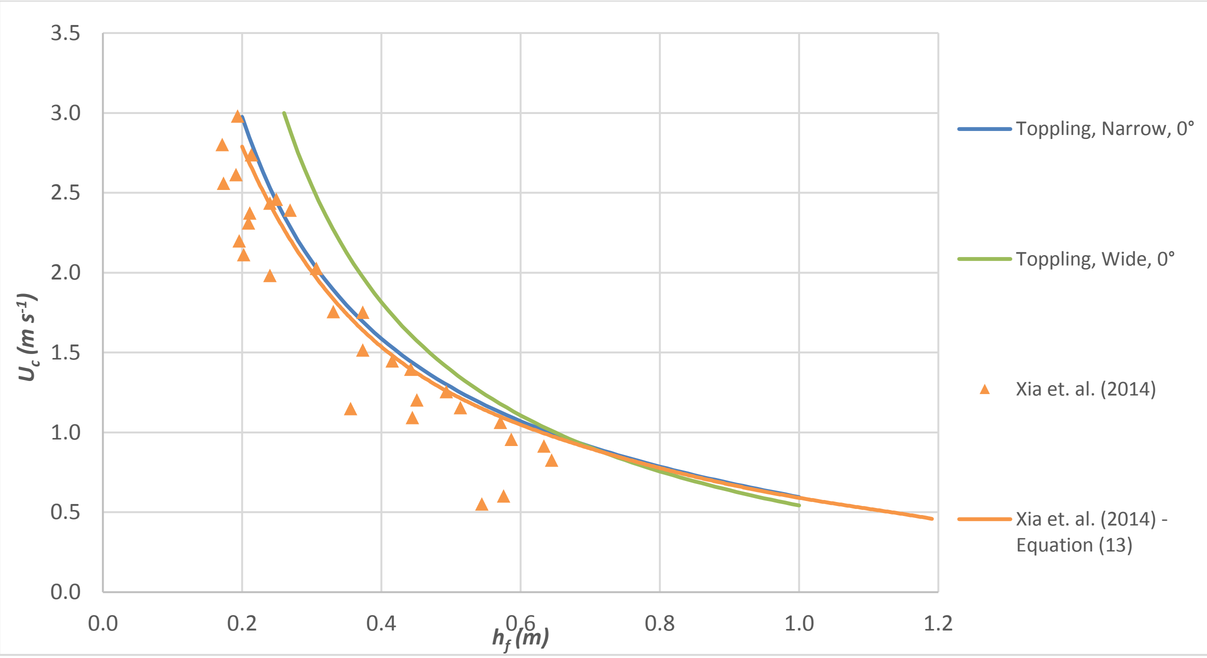

Figure 28 *Stability curve comparison between 0°, narrow and wide data sets from this experiment and the curve of Xia et. al. (2014).*

Both the shape of the curve and magnitude of the results compare well to Xia et. al. (2014), validating the methodology and apparatus used for this investigation.

It is useful to compare scale model data to that of real human subjects. Abt et. al. (1989) and Karvonen et. al. (2000) used real human subjects whilst Takahashi et. al. (1992) used scaled experiments. Their published data has been plotted against the experimental data from this study in Figure 29.

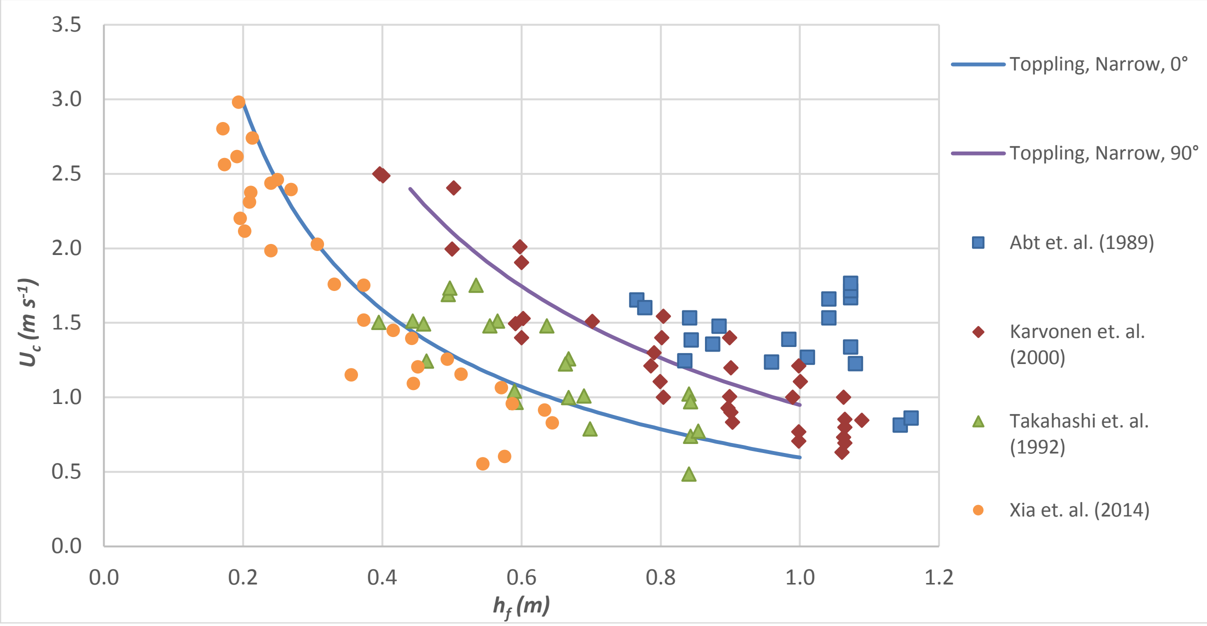

Figure 29 *Comparison of the experimental data (0° data sets) from this experiment to that of various previous human stability studies.*

It is expected that the scaled experiments conducted in this investigation will be more conservative than real human studies since real humans can adopt a more efficient posture.

Figure 29 shows that the scaled experimental studies underestimate the real human stability and can be over-conservative. The volunteers in both Abt et. al. (1989) and Karvonen et. al. (2000) were allowed to adjust their posture as they pleased.

Figure 29 shows that the orientation change from 0° to 90° produces much more similar results to those of Abt et. al. (1989) and Karvonen et. al. (2000).

4.3.5 Suggested Human Stability Criteria

Floodway flow may be incident on a human in any orientation or stance width. Therefore, a sensible approach to producing a stability criterion is to take the most conservative toppling stability curve, with a cut off above $U_c = 2.5$ ms^{-1} to account for the sliding failure mechanism. This will produce a stability curve, below which the floodway conditions will pose a low hazard to all postures.

Another stability curve can be produced based on the most stable orientation (e.g. wide, 90°), above which there would be a severe hazard to human stability in all orientations and stance widths. Following Xia et. al. (2014), an upper limit of 3 ms^{-1} for sliding was adopted. Combining the upper and lower bounds leads to the proposed human stability criteria, shown in Figure 30 (on the next page).

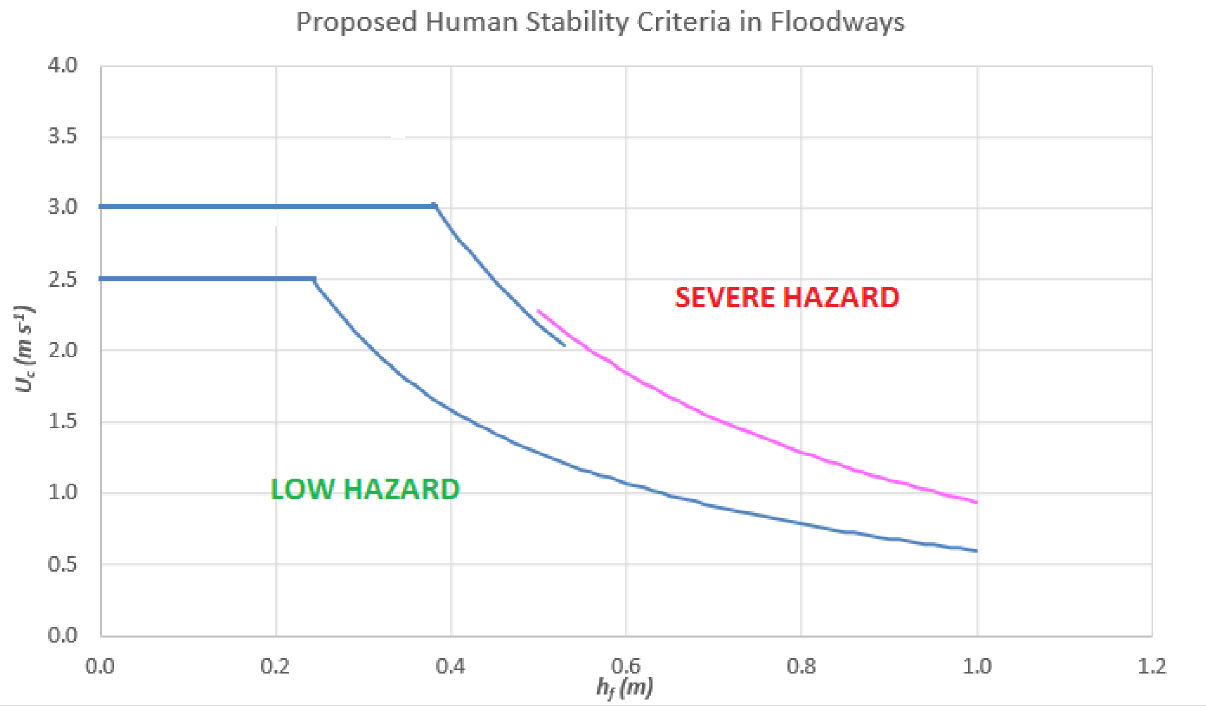

Figure 30 *The proposed human stability criteria in floodways.*

5 Experimental Accuracy and Sources of Error

There were a very large variety of factors capable of creating inaccuracy that were encountered during the course of this investigation. A separate brief section dedicated qualitative discussion is included here to improve the clarity of the preceding sections.

5.1 Discussion of Inaccuracies Present Both Experiments

5.1.1 Near Wall Effect

The Froude number (*Fr*) is defined as:

$$Fr = \frac{U}{\sqrt{\frac{gA}{B}}} \quad (33)$$

Where *U* is the flow velocity, *A* the channel area and *B* the flume width. For a Froude number greater than one the flow is supercritical, and subcritical if the Froude number is less than one. Froude number can be very simply calculated with the data recorded, doing so can reaveal the transtion from supercritical to subcritical flow for each results set. As the flow approaches the critical point, the beginning of the transition to subcritical flow can create a large "wave" in front of the models, especially in a narrow flume. This severly affects the ability to take depth and velocity measurements, as well as causing premature instability in the models.

Many of the figures with significant results gaps in the middle will have suffered from the near wall effect. A wider flume or smaller models are required if the wall effect hinders the experiment to the point that the results are unusable.

5.1.2 Measurement Errors

Depth measurements were taken with a needle depth gauge, with an accuracy of ±1mm. Velocity measurements were less accurate (see Section 3.2.1.2), therefore each time a reading was taken three times, with a mean value used. Figure 31 shows a representative spread of velocities for each data point.

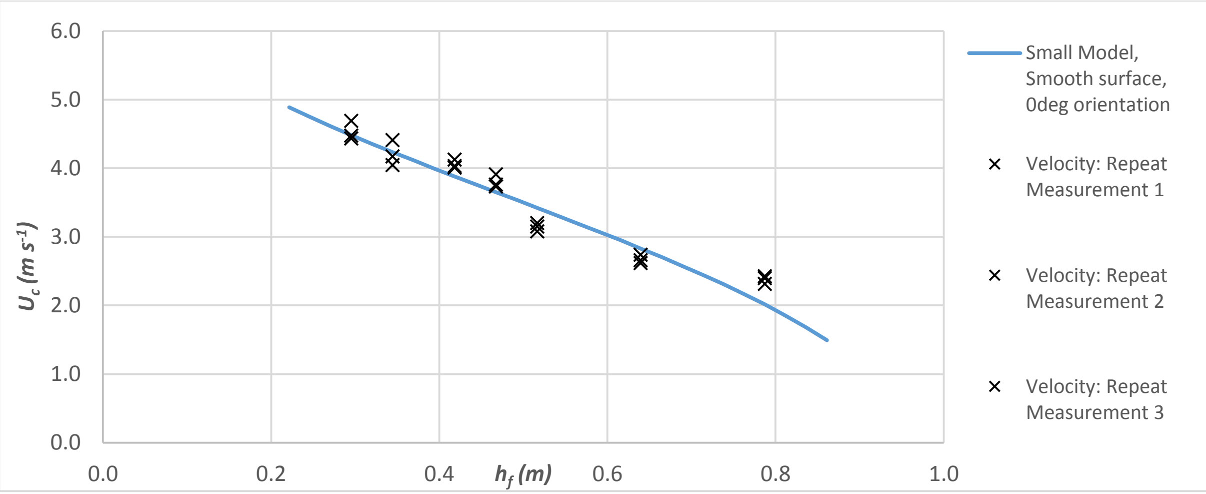

Figure 31 *Precision of velocity measurement.*

5.2 Discussion of Factors Affecting Vehicle Experiment Accuracy

Ground slope affects vehicle stability, Xia et. al. (2013) recorded a reduction in U_c of approximately 20% for a ground slope of 1:50 (which is an average estimate of ground slope for this study). Another factor affecting accuracy is that the depth water at critical instability in the vehicle experiments was generally less than 2cm, which makes finding the critical point difficult because the flow rate adjustment is not sensitive enough.

5.3 Discussion of Factors Affecting Human Experiment Accuracy

At high experimental velocity and depths in the flume (e.g. for the large model experiments), the flume is not long enough to allow unsteadiness to settle down in the working section, causing premature instability of the models. Also, scaled and static models cannot replicate the subtle complexity of the real human reaction to floods, again resulting in over conservative stability curves.

6 Conclusions and Further Work

Floods present a hazard to vehicles and humans, which can become unstable and be swept away. Recent flooding in Britain and globally, along with the predicted effects of climate change, have highlighted the need for more research into the effects of flooding. The primary aims of this experiment were to investigate the stability of humans and vehicles in floodways.

To investigate vehicle stability, a theoretical approach based on a sliding mechanism was first undertaken. To supplement this a laboratory experiment using three scale model vehicles in a water flume was carried out, to determine the free parameters produced by the theoretical analysis. More extensive investigation into bed friction and orientation was carried out than in any previous published studies. Conclusions from the investigation include the following:

1. Scaled stability curves for three different sized model vehicles proved to be similar for vehicles that displayed shape similarity, justifying the dimensional analysis and scaling method used.
2. An investigation into the effect of bed friction showed that the experimental results aligned with the theoretical analysis, where velocity changes with the square root of the friction coefficient ratio.
3. Investigating the effect of changing the vehicle orientation proved that the 0° and 180° were most stable, followed by the 45° and 135° orientations (which were similar).
4. The stability curves produced were shown to agree with those published by Xia et. al. (2013), however disagreed with Keller and Mitsch (1993) due to differences in the methods used.
5. A stability criterion for vehicles in floodways was produced, split into areas of low hazard and severe hazard, based on the results of this investigation and previous studies into vehicle stability.

There are numerous opportunities for further work on the stability of vehicles. Firstly, an investigation needs to be conducted into the effect of ground slope on stability, and its combined effects with friction coefficient and orientation considered. Stability in the presence of solitary waves should be investigated to gain insight into the potential effects of devastating events like tsunamis. The rolling failure mechanism should be investigated in combination with surface obstacles such as kerbs or bollards. Finally there are opportunities to investigate the stability of more varied vehicles, such as vans and buses, and the potential for an investigation into moving vehicles.

The second part of the study looks into the stability criteria for humans in floodways, a more complex theoretical and experimental study was undertaken using the same methodology as that used for the vehicle stability study. An investigation into the effects of posture on human stability was conducted, which builds on previous studies where posture was not specifically considered.

1 Separate stability curves were derived for sliding and toppling failure mechanisms, and the free parameters calibrated with the experimental data obtained.
2 Two different sized models, displaying geometric similarity, produced similar stability curves to each other and Xia et. al. (2014), (with a maximum difference in critical velocity of 20% for a given height) validating the experimental procedure, apparatus and scaling method.
3 An extensive investigation into the effects of posture on human stability was considered, where the effects of orientation and stance width were systematically considered. Increasing the stance width was found to have a small effect on stability in most orientations (approximately 10% increase in critical velocity for a given height), discussion of this can be found in the report. Changing the orientation had a much larger effect on stability, mainly due to the changing normal projected area. The difference in stability from a 0° to 90° orientation was found to be an increase of approximately 40% in critical velocity.
4 The stability criterion proposed by this investigation was found to be closer to the previous studies using real human subjects than the previous scale model studies, as a result of the posture investigation.

Further work could build on the study, investigating solitary waves and the effects of unsteadiness on stability would be two potentially large fields of study. An interesting strand of future investigation would be on humans attempting to move in floods, although this may require the use of real human volunteers to produce accurate results.

7 Bibliography

Abt, S. R., Wittier R. J., Taylor A., Love D. J., (1989), Human Stability in a High Flood Hazard Zone.

Athukorala P. C., (2012), Indian Ocean Tsunami: Disaster, Generosity and Recovery.

Bonham A. J., Hattersley R. T., (1967), Low Level Causeways.

Chanson H., (2004), The Hydraulics of Open Channel Flow: An Introduction, 2nd Edition.

Chien N., Wan Z. H., (1999), Mechanics of Sediment Transport, *American Society of Civil Engineers.*

Drillis, R., Contini R., Bluestein M., (1964), Body Segment Parameters, Found online at (available May 2015): http://oandplibrary.com/al/pdf_raw/1964_01_raw.pdf#page=48

Flack K. A., Schultz M. P., Review of the hydraulic roughness scales in the full rough regime, (2010).

Guo Q. S., Wang Y. H., (1995), Ergonomics.

Intergovernmental Panel on Climate Change (IPCC), (2007), Climate Change 2007: Impacts, Adaption and Vulnerability.

Jonkman S. N., Vrijling J. K., (2008), Loss of life due to floods, *Journal of Flood Risk Management.*

Karvonen R. A., Hepojoki H. K., Huhta H. K., Louhio A., (2000), The use of Physical Models in Dam Break Analysis.

Keller R. J., Mitsch B., (1993), Safety Aspects of the Design of Roadways as Floodways, *Research Report No.69.*

Lind N., Hartford D., Assaf H., (2004), Hydrodyanmaic Models of Human Stability in a Flood

Ludema K. C., Physical factors in tyre traction (1975), *Physics in Technology.*

Naulluri C., Featherstone R. E., Civil Engineering Hydraulics, 4th Edition (2001), pg. 180 – 184.

New South Wales Government: Dept of Environment and Climate Change, (2007), Floodplain Risk Management Guideline – Floodway Definition. Found online at (available May 2015): http://www.environment.nsw.gov.au/resources/FRMGuidelineFloodwayDefinition.pdf

Shand T. D., Smith G. P., Cox R. J., Blacka M., (2011), Development of Appropriate Criteria for the Safety and Stability of Persons and Vehicles in Floods.

Takahashi S., Endoh K., Muro Z. I., (1992), Experimental Study on People's Safety Against Overtopping Waves on Break-waters.

Xia J. Q., Teo F. Y., Lin B. L., Falconer R. A., (2011) Formula of incipient velocity for flooded vehicles, *Nat Hazards.*

Xia J. Q., Falconer R. A., Xiao X., Wang Y., (2013) Criterion of vehicle stability in floodwaters based on theoretical and experimental studies, *Nat Hazards.*

Xia J. Q., Falconer R. A., Wang Y., Xiao X., (2014), New Criterion for the Stability of a Human Body in Floodwaters

Appendices

A – Risk Assessment Retrospective

The apparatus used in this project did not change substantially throughout the year, in this respect the initial risk assessment submitted at the start of the year was fairly accurate and the broad hazards were the same. This project was almost entirely laboratory based using a small flume situated in the hydraulics laboratory, which presented a variety of hazards:

1. Working with water: presenting slip hazards, electrical hazards (electrical risks were very well managed around water), potential damage to nearby equipment and risk of disease if the water is not replaced regularly enough. Towards the end of the experiment, the water wasn't particularly clean, and equipment wasn't available to clear spillages. Water could have been replaced more regularly and especially before periods of experiments with high levels of water contact (for example the high velocity human stability experiments, where the model would have to be retrieved from the bottom of the end tank every time).
2. Trip hazards: the confined laboratory area presented many trip hazards, very special care was needed to manage the hazards. Ideally the flume would be situated in a more spacious area, but this was not available and the risks of a confined area could be mitigated effectively.
3. Working at height: the flume required the use of small stands approximately 0.5 m high to position the models. Again, special care was needed when on the stands.

B – Acknowledgements

Thanks go to my supervisor, Dr Dongfang Liang, who provided great support throughout all aspects of the project. I would also like to thank the workshop technicians Roy and Rob who provided knowledge and support as well as setting up the apparatus.